Comparison of Traditional Two-Spool and Three-Spool with Vaneless Counter-Rotating Low-Pressure Turbine for Aircraft Propulsion Power Extraction

by

Luke Michael Burgett

A Thesis Presented in Partial Fulfillment
Of the Requirements for the Degree
Master of Science

Approved April 2019 by
Graduate Supervisory Committee

Timothy Takahashi, Chair
Werner Dahm
Steven Trimble

ARIZONA STATE UNIVERSITY

May 2019

ABSTRACT

In previous work, the effects of power extraction for onboard electrical equipment and flight control systems were studied to determine which turbine shaft (i.e. high power shaft vs low power shaft) is best suited for power extraction. This thesis will look into an alternative option, a three-spool design with a high-pressure turbine, low-pressure turbine, and a turbine dedicated to driving the fan. One of the three-spool turbines is designed to be a vaneless counter-rotating turbine. The off-design performance of this new design will be compared to the traditional two-spool design to determine if the additional spool is a practical alternative to current designs for high shaft horsepower extraction requirements. Upon analysis, this thesis has shown that a three-spool engine with a vaneless counter-rotating stage has worse performance characteristics than traditional two-spool designs for UAV systems.

DEDICATION

To my parents whom without I never would have been able to pursue my passion and encouraging me to further my education.

TABLE OF CONTENTS

Page

CHAPTER Page

LIST OF TABLES

LIST OF FIGURES

Figure Page

Figure Page

Figure Page

Figure Page

NOMENCLATURE

Symbol		Page
h	Specific Enthalpy (Btu/lbm)	6
g	Gravitational constant 32.17(ft/s^2)	6
J	Mechanical equivalent of heat 778.2 (ft-lbf/btu)	6
U	Mean section blade speed (ft/s)	6
R_o	Rotational Ratio	6
φ	Flow coefficient	6
C_1	Pitchline velocity at rotor inlet (ft/s)	6
$\propto_1$	Absolute flow angle at rotor inlet (deg.)	6
T	Thrust (lbf)	10
$\dot{m}_i$	Inlet core mass flow (slugs/s)	10
V_i	Inlet velocity (ft/s)	10
$V_{e,core}$	Core exit velocity (ft/s)	10
$V_{e,bypass}$	Bypass exit velocity (ft/s)	10
f	Fuel to air ratio	10
$A_{e,core}$	Core exit area (ft^2)	10
$A_{e,bypass}$	Bypass exit area (ft^2)	10
P_i	Inlet static pressure (lbf/ft^2)	10
$P_{e,core}$	Core exit static pressure (lbf/ft^2)	10
$P_{e,bypass}$	Bypass exit static pressure (lbf/ft^2)	10
BPR	Bypass ratio	10

Symbol		Page
$\dot{w}$	Specific work (Btu/lbm)	11
C_2	Pitch line velocity at rotor exit (ft/s)	11
$\propto_2$	Absolute flow angle at rotor exit (deg.)	11
w_1	Pitch line relative velocity at rotor inlet (ft/s)	12
w_2	Pitch line relative velocity at rotor exit (ft/s)	12
$C_{1,x}$	Pitch line axial velocity at rotor inlet (ft/s)	20
β_1	Relative flow angle at rotor inlet (deg)	20
β_2	Relative flow angle at rotor exit (deg)	20
R_x	Degree of reaction	20
$C_{1,y}$	Pitch line tangential velocity at rotor inlet (ft/s)	20
$C_{2,y}$	Pitch line tangential velocity at rotor exit (ft/s)	20
R	Specific Gas Constant of Air 53.38(ft*lbf/lbm/°R)	20
T_{T4}	Combustor exit total temperature (°R)	38
T_{T5}	Turbine exit total temperature (°R)	38
P_{T4}	Combustor exit total pressure (lbf/ft^2)	38
P_{T5}	Turbine exit total pressure (lbf/ft^2)	38
γ	Ratio of Specific Heats	38
η_T	Isentropic Efficiency	38
N	Shaft revolutions per minute	56
τ	Torque (ft*lbf)	56

Chapter 1: Introduction

Unmanned (UAV) systems may fly with complex electronic packages that require more power to operate than other typical general aviation aircraft. Commercial off the shelf engines generate power for onboard systems from alternators driven by the primary turbine shafts. Alternatively, the aircraft may use a separate power source such as batteries or another gas turbine (i.e. an auxiliary power unit) to power the onboard systems. Recent research has focused on how to determine which turbine shaft is best suited for power extraction and the performance penalties for doing so [1]. Although the power required for onboard systems varies from aircraft to aircraft, it is typically magnitudes smaller than the power required to drive the compressor (anywhere between 1%-0.1% for manned aircraft [2]). This study investigates the possibility of adding an extra turbine stage that decouples the power extraction used for onboard systems from the rest of the engine.

Vaneless counter-rotating (VCR) turbines have been an area of study in the past starting in 1910, with the most significant modern work on the subject coming in the 1980's [3]. The premise behind VCR turbines is that the length of the turbine can greatly be reduced by eliminating the stator vanes that are typically found between each blade row. The stators are needed to turn the flow from the previous stages since the flow is now going the opposite direction from the blade. If the flow was not turned the flow from the previous stage would impede the movement of the next blade row. If consecutive blade rows were to rotate in opposite directions to one another it renders the need for stators unnecessary seen in Figure 1. This helps shorten turbines while reducing material cost. It does increase the complexity of the

turbine because an outer shaft that encompasses the entire turbine is required for multi-stage turbines.

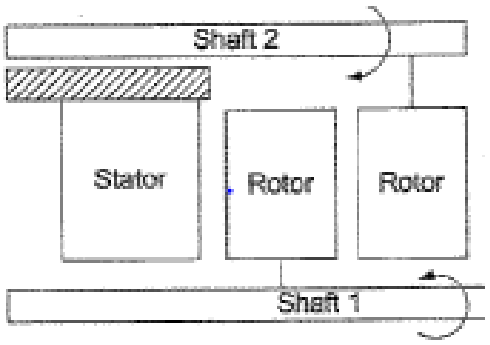

Figure 1: Vaneless Counter-rotating Turbine Concept [3]

Based off previous research published by Stone & Takahashi [1], it appears that the shaft driven by the low-pressure turbine is better suited for power extraction than the high-pressure turbine. The proposed design studied in this thesis investigates what the performance would be if the power extraction was taken from the intermediate low-pressure turbine or the fan turbine of a three-spool engine. This proposed design will have one VCR stage for the low-pressure turbine which will help minimize the size difference between the two designs. This paper will not be looking at the cost of materials or the structural limits of the turbine; it will focus more on the aerodynamic design of the VCR turbine and its affect on performance.

Chapter 2: Literature Review

Papers published discussing VCR models emphasize that such turbines can reduce the weight and length on engines because the technology eliminates stator vanes. A VCR can allow the engine designer to heavily load each stage of the turbine. [3].

The F119 engine designed by Pratt and Whitney and used in the F-22 fighter is the sole production engine using a VCR. [4]. The lack of production type engines means that few fully built VCR engines have been compltely tested and those that have are highly protected for thier proprietary technology.

2.1: Structural Considerations

For the counter-rotating portions of the turbines the blades do not expereince the typical tensile loads that conventional turbine blades expereince; rather, they experience compressive forces. An analysis done by the Chinese Academy of Sciences discusses the stress expereinced by these counter-rotating sections. [5]. The stresses are greater since more of the blades are at a larger radius and experience larger centrifugal forces. [5]. Another article suggests building blade disks out of ceramics as they are better suited for compressive forces. [3].The additional benefit of building blades and disk out of ceramics is the increased maximum temperature at which they are able to function at when compared to traditional alloy based blades. There is yet to be a clear consensus on how such blades and disk should be made as few VCR turbines have been produced.

2.2: Thermal Considerations

VCR turbines are susceptible to many of the same thermal loads that traditional turbines experience. If the blades exceed limit temperatures, they can crack, warp or break off. Some authors have noted a difference with the heat transfer coefficients for VCR turbines; most notably the VCR leading edge will experience lower heat transfer coefficients.to a traditional turbine blades; see Figure 2. [3]. Even though VCR turbines may have a lower heat transfer coefficient they are affected by the hot streaks; see Figure 3. These hot streaks temperature can vary between 10%-20% of the average inlet temperature [6] these hot streaks can be seen in Figure 3 on the next page. The performance of a VCR degrades as the hot streak temperature increase as they affect the relative Mach number across the blade. [7]. When the relative Mach number is changed the relative blade angles coming off the stage changes. When this occurs, the flow may be at such an angle that the flow separates once it reaches the next VCR if no stator vane exists to align the flow.

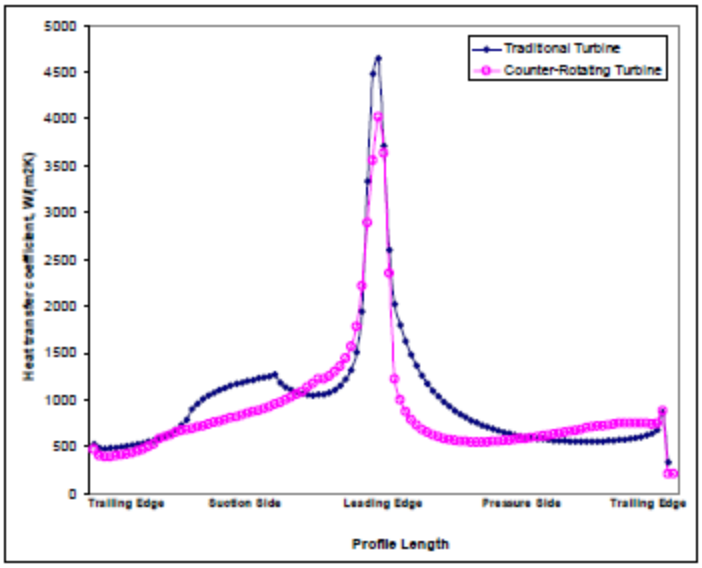

Figure 2: Heat Transfer Coefficient for Traditional and VCR Turbine [3]

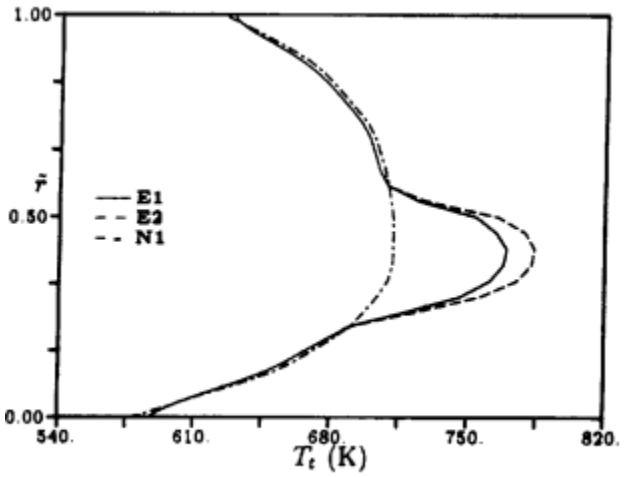

Figure 3: Total Temperature Distribution after Rotor Stage that Experiences Hot Streaks

2.3: Aerodynamic Considerations

Prior research notes that VCR turbines are far more capable and efficient when their blades are highly loaded. [8] [9]. LuCheng [9] and Moroz [3] noted that VCR turbines are insensitive to

various total-to-static pressure ratios as they vary from the "design point". There is a discrepancy between these two works though. LuCheng [9] varies only backpressure while maintaining a constant rotation speed ratio. While the work done by Moroz [3] and his peers change both the rotation speed ratio and backpressure at the same time. The work done by Moroz [3] states that in all cases that the VCR turbine outperforms traditional turbines when it comes to total efficiencies [3] as seen in Figure 4. Research published by Wintucky & Stewart [8] back in 1958 produced similar results with the VCR turbines outperforming traditional turbines when highly loaded with their results seen in Figure 5. LuCheng, on the other hand, produces results that contradict the previous work and show that VCR are better at constant rotation speed ratios, but are extremely sensitive and have poor performance when their rotation speed ratio (R_o) are changed [9]. The results Wintucky & Stewart [8], Figure 5, show that as the VCR stage blade speed is reduced the overall efficiency out-performs a traditional design. Equation 3 represents the work speed parameter used in Figure 4. This supports the results Lucheng findings at low rotational ratios, Equation 1.

$$R_o = \frac{U_2}{U_1} \tag{1}$$

$$\varphi = \frac{C_1 \cos \alpha_1}{U_1} \tag{2}$$

$$\lambda = \frac{U^2}{g * J * \Delta h} \tag{3}$$

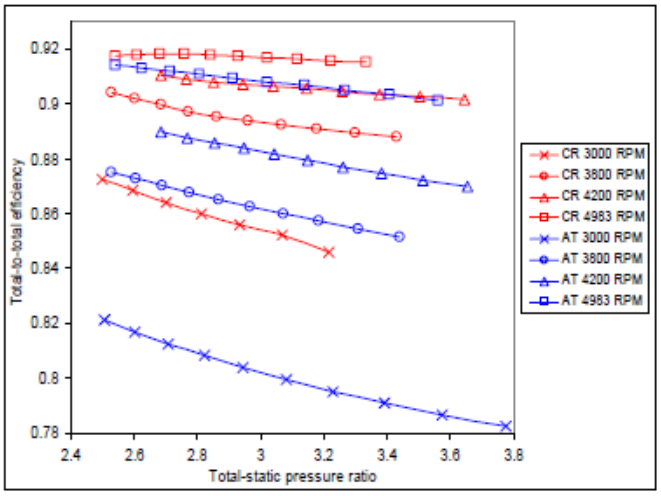

Figure 4: Off-design Comparison for Various Rotational Speeds and Total-static Pressure Ratios [3]

In general VCR turbines outperform standard turbines when the rotation speed ratio is small i.e., when the VCR stage is rotating at lower speeds. The low rotation ratio helps insure that the work speed parameter will be low by keeping the VCR blade speed is low. The low flow coefficient, φ, (see Equation 2) stated in LuCheng's research corresponds to the flow leaving the blade row before the VCR blade row. The low flow parameter means that the flows axial velocity is low compared to the blade speed of the non-VCR blade row. The flow will therefore have a large tangential flow component and enables more work to be extracted from the flow. Chapter 3 will discuss how a larger tangential velocity enables higher power extraction.

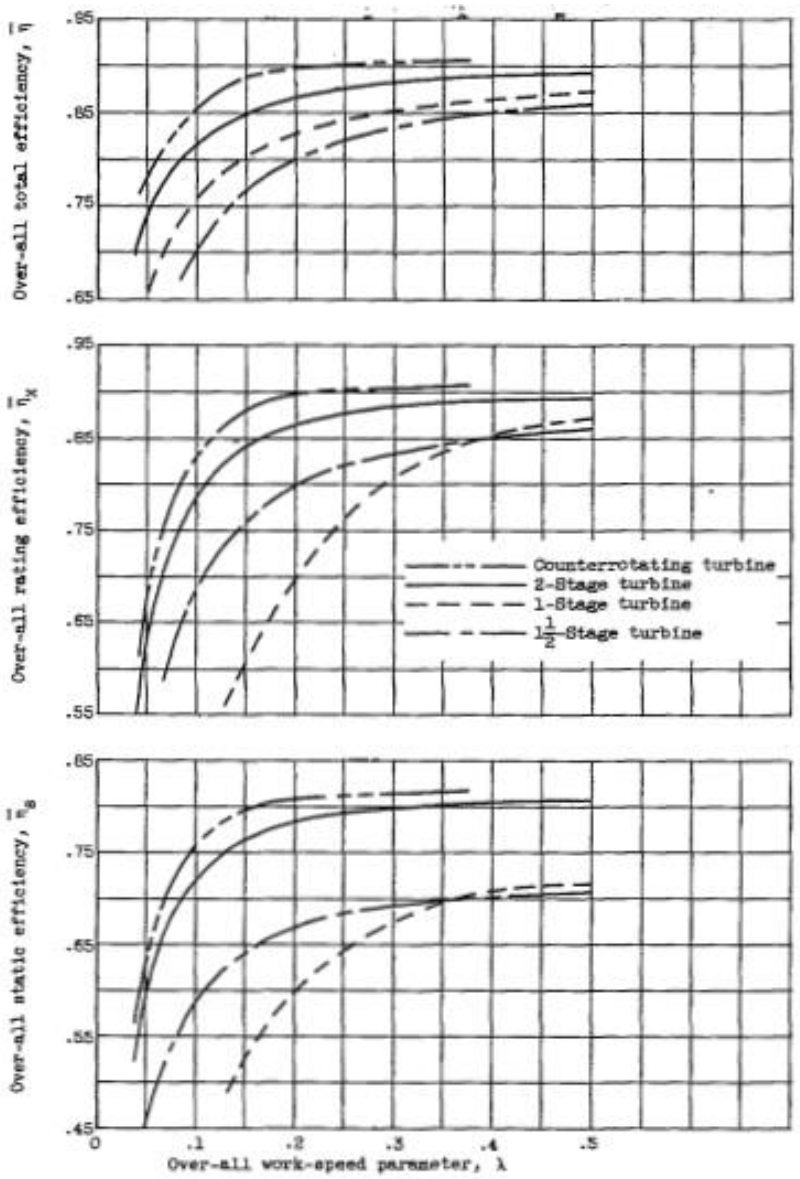

Figure 5: Efficiency Comparison for Various Work Speed Parameters [8]

Chapter 3: Gas Turbine Fundamentals

Jet engines are a continuous flow system that operates using the Brayton cycle to produce both shaft work and thrust. The thrust for a turbofan engine is given by Equation 4 using the conservation of mass through a control volume. A typical two-spool turbofan engine is depicted in Figure 6 below.

$$T = \dot{m}_i * \left((1+f) * V_{e,core} - V_i + BPR * V_{e,bypass}\right) + A_{e,core} * \left(P_{e,core} - P_i\right) + A_{e,bypass} * (P_{e,bypass} - P_i) \quad (4)$$

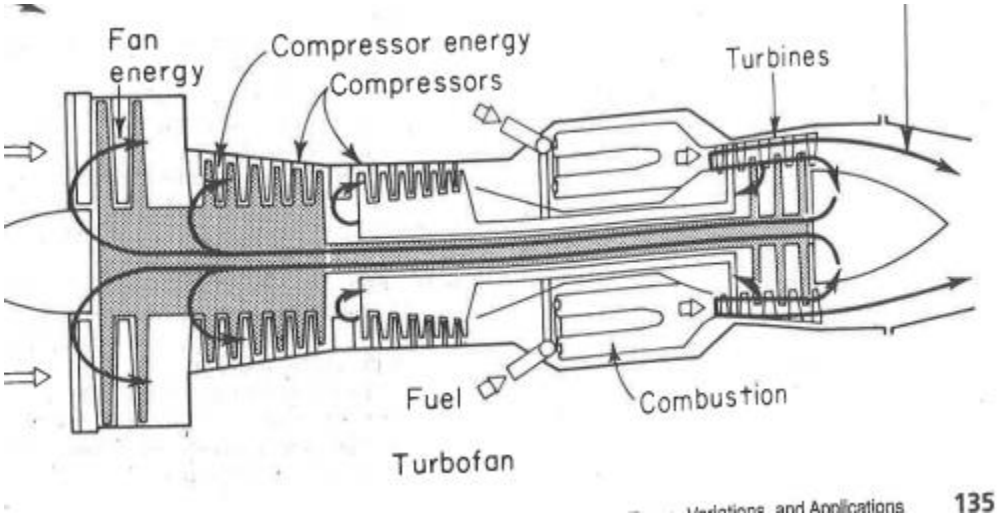

Figure 6: Generic Two-spool Turbofan Engine [10]

The Brayton cycle converts chemical energy that is added to the flow in the combustor into shaft work in the Turbine, which powers the compressors and the fan, and the excess energy is then turned into velocity in the nozzle.

There are four distinct phases in the Brayton cycle and they are as followed isentropic compression (0→3), heat addition at constant pressure (3→4), isentropic expansion (4→8), and finally heat removal at constant pressure (8→0). Figure 6 shows the *T*-*s* diagram for an ideal Brayton cycle along with which components of the jet turbine belong to each phase of the cycle. For this thesis the station numbering used will be the same as presented in Figure 7.

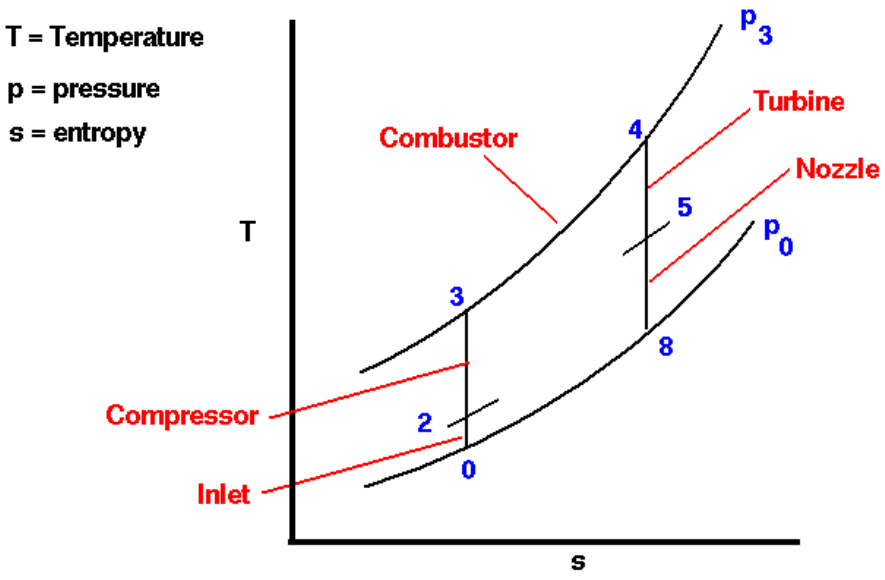

Figure 7: Ideal Brayton Cycle Temperature vs Entropy (*T*-*s* diagram) with Station Labels [11]

Jet engines only affect the first phases (0→8) of the Brayton cycle. The inlet, fan, and compressors are linked to the first phase, the combustor is the second phase, and the both the turbines and nozzles are linked to the expansion phase.

The compression phase is done in two ways. The first is the inlet/diffuser that increases the pressure in the system by slowing the flow from flight conditions down. The total pressure does not change in this stage only the static pressure increases. The compressors impart work to the flow. For an axial flow compressor flow passes through numerous airfoil shaped stator and rotor blade rows. In compressors, the flow speed increases through the rotors therefore increasing the kinetic energy of the system, Equation 5. Figures 8 and 9 show the flow absolute velocity and relative velocity vectors with respective angles that are used in Equation 5. The stators then convert that extra kinetic energy into potential energy (i.e. total pressure increases) by slowing the flow back down to speed the flow had originally had when entering the rotor both of these processes are done isentropically in the ideal case.

$$\dot{w} = U * (C_2 \sin \alpha_2 - C_1 \sin \alpha_1) \tag{5}$$

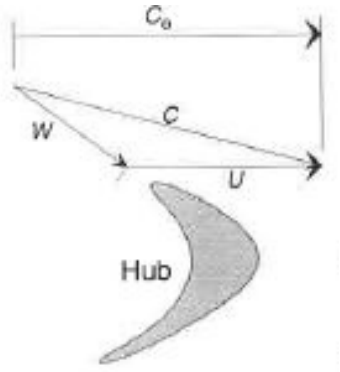

Figure 8: Vector Diagram for Rotor Inlet [12]

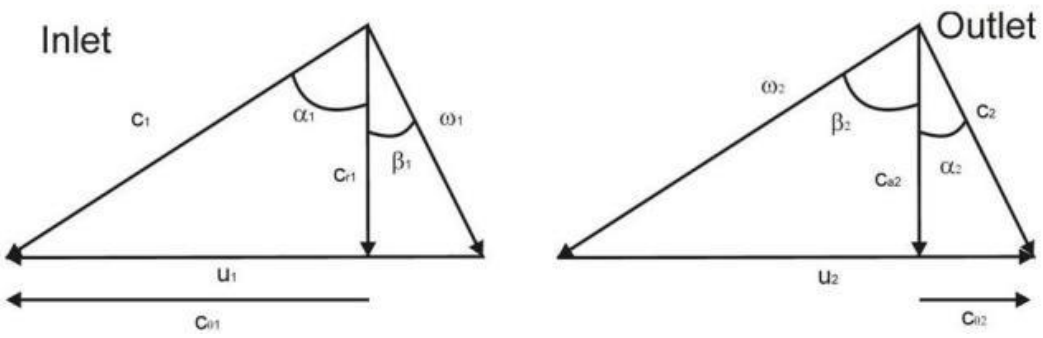

Figure 9: Vector Diagrams for Rotor Inlet and Rotor Exit with Angles Shown [13]

Once the desired pressure has been obtained, heat is added to the flow. This is done by adding fuel and igniting the air and fuel mixture. The static pressure is held constant during this process.

The turbines isentropically extract work from the flow by removing the heat from the flow using the same principals as the compressors, but instead of imparting work to the flow turbines extract work reducing the kinetic and potential energy of the flow. The nozzle then speeds up the flow leaving the turbines. Nozzles do no work to the system; the total pressure and temperature ideally remain constants. The nozzle attempts to speed up the flow so that the static pressure at the nozzle exit is the same as the free stream velocity.

The processes described earlier assume isentropic expansion and compression for both the inlets, compressors, combustor, turbines, and nozzles. This never is the case in the real world. Certain irreversibilities are added to the flow in each phase that lowers the overall performance of an engine, a realistic Brayton cycle is seen in Figure 10. Improving these steps in the cycle to resemble isentropic flow is a goal of numerous research institutes and businesses. Vaneless

counter rotating turbine stages is a way of doing this by eliminating the need for stator vanes. Stator vanes added irreversibilities to the process due to skin friction across the surface, Vortex dissipation due to tip clearances, boundary layer separation, etc. Though the stator vanes do not do any work and the irreversibilities they introduce are small, they are not necessary to the system if VCRs are used and by removing them the irreversibilities in the turbine stage is reduced.

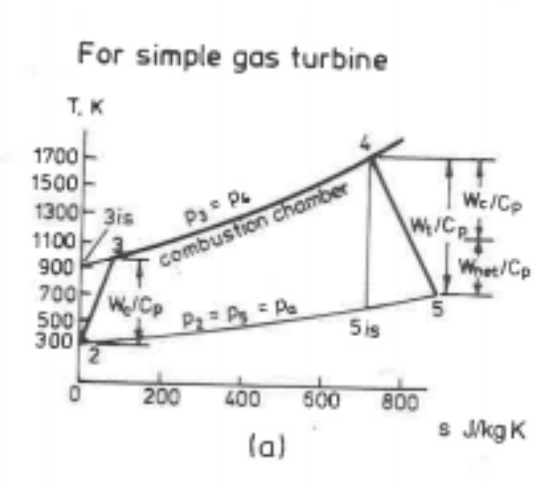

Figure 10: Realistic Brayton Cycle with Irreversibilities Included

The performance of both turbines and compressors are highly dependent on their blade angles and the speed at which they rotate as seen in Equation 5. The blade speed U is directly related to the RPMs of the turbine and so are the absolute angles coming off the rotor. To determine the efficiency and pressure ratios of compressors and turbines they must be thoroughly tested to determine the performance of them. The testing results in compressor and turbine maps as seen in Figures 11 and 12 on the next page. These maps are critical to any engine design.

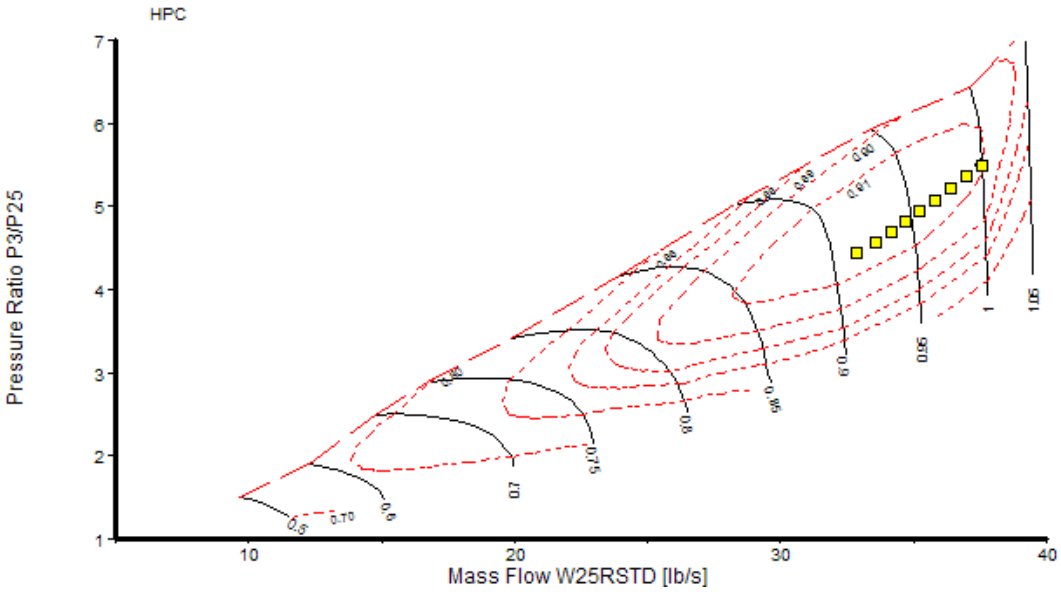

Figure 11: Generic Compressor Maps with Normalized Speed Lines [14]

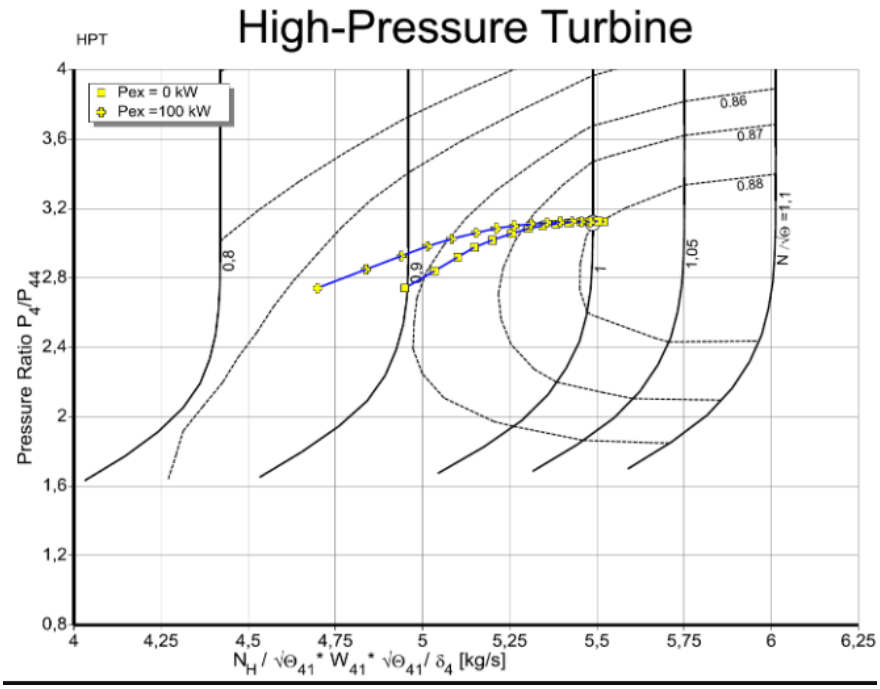

Figure 12: Generic Turbine Map with Normalized Speed Lines

Chapter 4: Problem Overview

UAV systems are smaller than commercial aircraft, and use smaller gas turbine engines to provide the thrust and power they require to fly and operate. These smaller gas turbines typically have lower performance when compared to larger engines because their size limits some of the technologies that can be fitted within them. Vaneless counter rotating systems are a technology that can be fitted into these smaller engines to help improve on the efficiency by reducing the length of the engines and eliminating the stator vanes.

For this thesis, a nominal UAV, was used as an aerodynamic reference; see Figure 13. The turbofan engine was sized and configured to meet the requirements of this UAV system. Two separate turbines were considered: one that follows a traditional two-spool set up and the second design that incorporates the vaneless counter rotating technology along with a three-spool configuration.

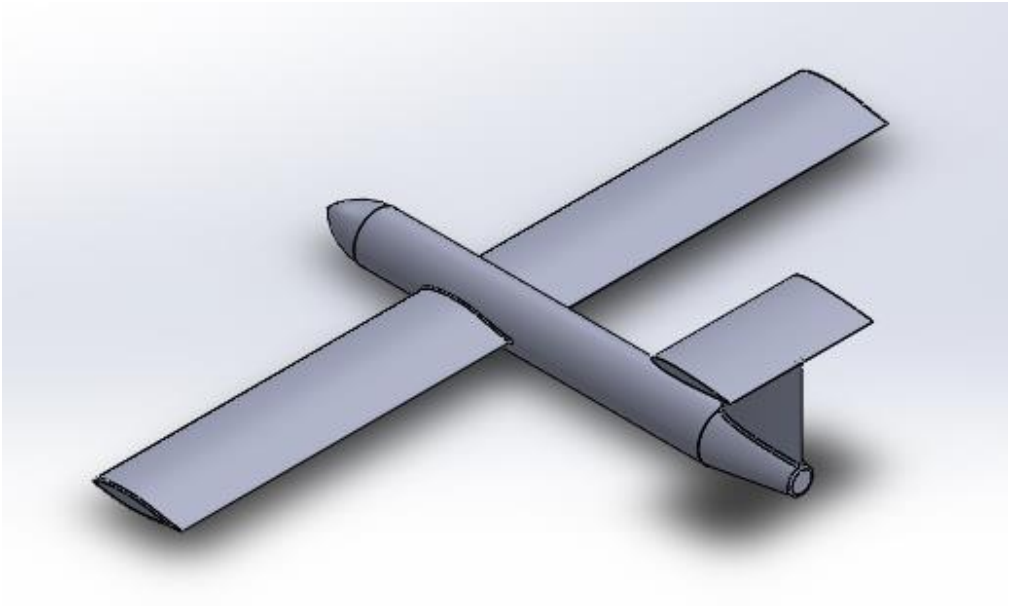

Figure 13: Nominal UAV Engine Models Designed to Power

These two designs are both optimized for high efficiency at the same altitude, Mach number, and thrust requirement. The off-design performance of both engines may be compared; “five column” performance data is generated and interacted with the nominal UAV aerodynamics. This five column data is used to for creating a flight envelope for the UAV system which allows for a comparison between the two design models.

Both turbofan configurations are compared for various power extraction settings as well. UAVs typically fly with large onboard electrical power demands. To test this, the models analyzed at 0, 50, and 100 shaft horsepower extraction. The reason behind selecting such power demands is they are well above the 0.1%-1% that commercial aircraft require and will likely push realistic maximum power demand a UAV would ever require.

They key performance variables for this systems analysis includes the specific range, thrust specific fuel consumption, and the design point isentropic efficiency. The design point isentropic efficiency is the primary concern of engine designers since this is the designated speed, altitude, and thrust level that the aircraft will fly at and spend the majority of the engine’s life at. The specific range is important as it tells the aircraft designers and pilots at what is the “best” speed and altitude the UAV should fly at to maximize range.

Chapter 5: Programs Used

To perform this study, multiple programs were needed to build a complex model and compare the performance of each engine design.

5.1: Installed Engine Performance

To compare technolgies, each engine was sized to develop 450-lbf thrust at 30,000-ft ISA flying at Mach 0.4. NASA's Numerical Propulsion System Simulation (NPSS) is an aerothermomechanical simulation program that is said to accuratly model the interaction between all the components in a gas turbine engine for design point and off-design point flight conditions. [15] NPSS comes with multiple examples and also provides compressor maps which are difficult to acquire to their proprietary nature. The *TurboFan* model provides both a high pressure, low pressure, and fan compressor maps. They were scaled down to the bypass ratio, mass flow, and thrust at the desired altitude and Mach number.

The turbine stages were created using other programs. The data generated in the following programs was then filtered to create similar data sets that NPSS uses. I created new turbine maps for the high pressrue tubrine (HPT), the low pressure turbine (LPT), and fan power turbine (FANT).

The default maps were used at first to obtain the inlet conditons such as the mass flow, total pressure, and total temperature at the exit of the combustion chamber. These conditions do not change when new turbine maps are created as they come before the turbines and are independent of the turbines at the design point.

The overall pressure ratio, OPR, of 17 was chosen as it is a typical pressure ratios for small engines. The fan pressure ratio was selected to be 1.7, typical of medium BPR turbofans; low-pressure compressor pressure ratio to be 2.0 and the high pressure compressor pressure ratio to be 5.0 .

The turbine inlet temperature was set to be 2100°R as this is below the melting temperature of standard turbine blade materials that way no special cooling would be need and to help simplify the model. A bypass ratio, BPR, of 4 was selected as ultra-high bypass ratios are atypical in smaller gas turbine engines. The flight conditions chosen was a flight Mach speed of 0.4 at an altitude of 30,000ft ISA. The altitude chosen means it can operate in most environments and at safe distances for recconissance missions. The slower Mach number was chosen for longer loitering times over select target areas.

Based off these design point flight conditions NPSS calculated that the mass flow through the core of the engine would be approximately 4.0 lbm/s and the total pressure at the inlet of the turbines would be 78.7 psi (this is assuming a 5% total pressure drop across the combustor). The core inlet size for the engine was calculated to be roughly 10 inches in diameter and is a starting point for the turbine sizing. Based on the information above the power required for the Fan was

537.19 Hp, the low pressure compressor was 173.85 Hp, and the high-pressure compressor was 576.92 Hp. These conditions are then used in the next programs to begin developing each of the turbine stages.

A vector diagram visualizer was programed and used to begin the initial calculations for the turbine [16] see Figure 14. The vector diagram tool assumes the flow is axial entering the turbine and maintains a constant axial velcoity throughout the entire turbine stage. The spread sheet calculates the meridional velocities and angles required to meet a specific power requirement for each stage. The tip and hub angles are also calculated assuming free vortex flow.

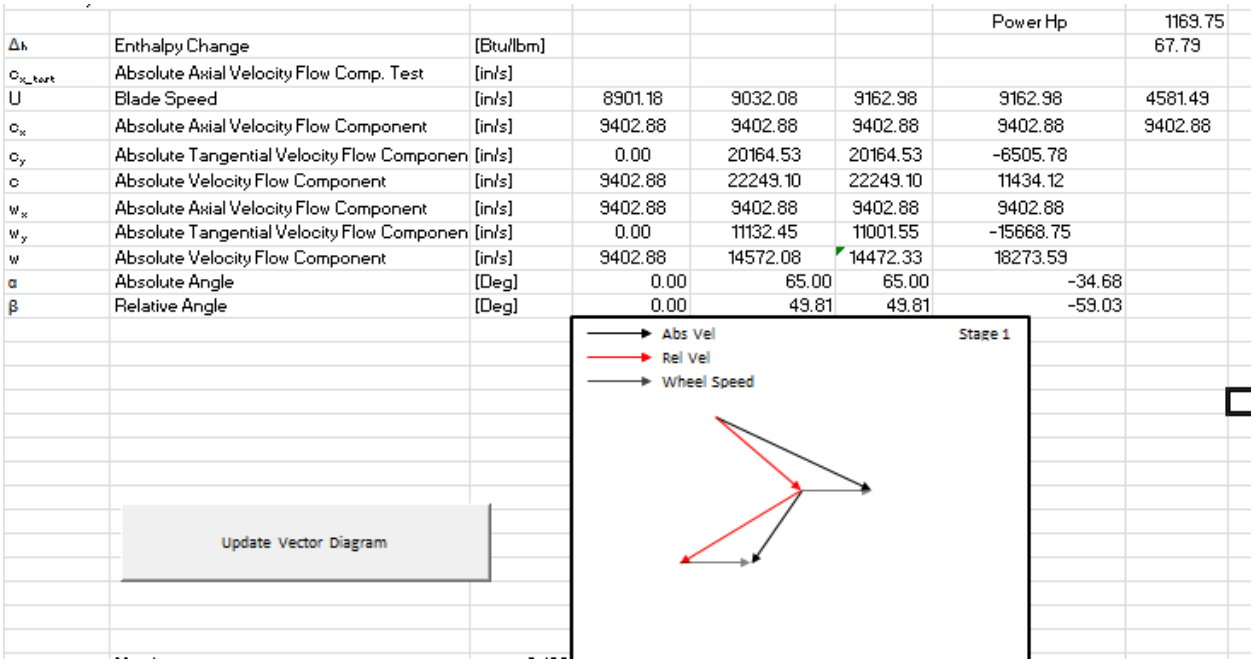

Figure 14: Velocity Vector Diagram Visualizer Using Arbitrary Conditions

The user of the program inputs the pressure and temperature of the flow at the inlet and the user changes the stator exit angle in each stage to achieve the desired velocity triangles. For this study approximatly 50% reaction was chosen for traditional stator rotors stages to achieve

relatively symmetric velocity diagrams to prevent large pressure drops across either the stator or rotor and minimize the likelyhood of flow separation.

The rotor exit angles are a function of the power required, blade speed, and stator tangtial velocity for each stage; Equations 6 & 7 shows the relation. The sizing of the turbine and the speed of the blades are the main design variables can an easily be changed to obtain the desired reaction. The counter rotating stage is designed as an impulse rotor since there is no stator and the pressure drop must be completely across the rotor.

$$C_{y,2} = C_{y,1} - \frac{P * 550 * g}{\dot{m} * U} \tag{6}$$

$$R_x = \frac{C_x}{2U} * (\tan \beta_2 - \tan \beta_1) \tag{7}$$

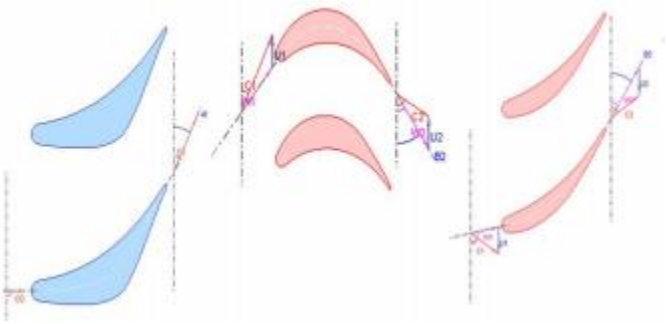

Figure 15: Vaneless Counter Rotating Velocity Triangles. Red Represents Blades Blue Represents Stators [3]

TD2 a NASA code was used to design turbines at the design point [17]. The program requies the total Hp for the system, the power split between stages, the turbine diameter at each section, the spacing between turbine blades, the inlet temperature, the inlet pressure and the stator exit

angles. The pressure, temperature, and power requirement came from the design point values that NPSS provided. The stator angles and stage diameter for the first iteration came from the velocity vector diagram tool.

```
     ASU 5Stg 3 Spool Model HPT model
          1                  0     0     0     0     0
&NAM1 NSPOOL=1 NAV=1 NLINES=3 GASC=53.38 FLWM=4.0
NLT=1 RLT=4.85 FAR=0.017
TOLT=2100. POLT=78.7 BETLT=0.0
&END
&NAM2 RPM=20000. HP=576.92 NSTG=2 FHP=0.5,0.5
XSTAT=-1.5,0.0,1.0,1.5,3.0,4.5,5.0 VISC=0.0000297
RANN(1,1)=7*4.5
RANN(1,2)=2*5.0,3*5.25,2*5.375 NXT=3 IWRL=2*1
RNXT(1,1)=4.5,4.75,5.0 RNXT(1,2)=4.5,4.85,5.25
WRL(1,1)=73.85,73.0,72.16
WRL(1,2)=71.5,68,64.5
IPOF=2*1
RSXT(1,1)=4.5,4.85,5.25
RSXT(1,2)=4.5,4.85,5.375
DVMDR(1,2)=3*0.0 DVMDR(1,4)=3*0.0
YOSS=3*0.99 YOSS(1,2)=3*0.99 YOSS(1,3)=3*0.99 YOSS(1,4)=3*0.99
&END
```

Figure 16: TD2 Three-spool High-pressure Turbine Input File

Due to the numerous input requirements the vector diagram inputs and results were used as a starting point for the program. TD2 then produces the required rotor angles, and stator inlet angles to meet the desired design point requirements. The program is used in an iterative process until an optimal point is reached. The program is limited when designing the VCR model. The program is unable to model two spools rotating in opposite directions. To over come this issue the VCR model was broken into three separate models one for each of the spools in the three-spool model.

NASA'S AXOD software which is specifically designed for off-design calculations of turbines is used to produce the off-design performance characteristics of both styles of turbines [17]. This program requires additional inputs compared to TD2, but the results from TD2 produce all the required data need to create the input files for the two styles of turbines. The program runs each design model at various mass flows at a constant RPM until the final blade row reaches chocked-flow conditions. The input files can handle multiple RPM inputs at once and quickly produce multiple data points that latered are turned interpolated into the required data for the NPSS turbine maps. The turbine maps in NPSS require the efficiency and corrected flow that correspond to pressure ratios at various RPM settings. An example of the interpolated data that was inputted into the NPSS model is shown in Figure 17.

Efficiency vs PR							
PR	120%	110%	100%	90%	80%	70%	60%
1.1	0.355	0.503	0.620	0.713	0.787	0.845	0.885
1.12	0.362	0.509	0.625	0.718	0.791	0.848	0.895
1.13	0.366	0.513	0.628	0.720	0.793	0.886	0.895
1.19	0.636	0.710	0.772	0.861	0.884	0.893	0.882
1.2	0.638	0.712	0.829	0.862	0.885	0.893	0.867
1.3	0.803	0.836	0.862	0.885	0.884	0.870	0.844
1.35	0.836	0.858	0.875	0.884	0.882	0.848	0.817
1.4	0.837	0.859	0.875	0.876	0.866	0.847	0.793
1.45	0.839	0.867	0.874	0.874	0.865	0.821	0.777
1.5	0.854	0.866	0.873	0.861	0.852	0.808	0.760
1.55	0.854	0.866	0.865	0.863	0.853	0.794	0.743
1.65	0.854	0.862	0.867	0.866	0.857	0.768	0.710
Corrected Flow vs PR							
PR	120%	110%	100%	90%	80%	70%	60%
1.1	2.423	2.421	2.421	2.421	2.422	2.423	2.426
1.12	2.431	2.430	2.429	2.429	2.430	2.432	2.848
1.13	2.435	2.434	2.433	2.433	2.434	2.849	2.851
1.19	2.858	2.858	2.859	3.199	3.201	3.202	3.204
1.2	2.860	2.860	3.199	3.201	3.202	3.204	3.496
1.3	3.499	3.500	3.502	3.753	3.755	3.757	3.759
1.35	3.753	3.755	3.757	3.759	3.760	3.980	3.982
1.4	3.758	3.760	3.762	3.980	3.982	3.984	4.000
1.45	3.763	3.980	3.982	3.985	3.987	4.010	4.000
1.5	3.971	3.984	3.987	4.024	4.019	4.011	4.000
1.55	3.970	3.988	4.025	4.025	4.020	4.012	4.001
1.65	3.970	4.022	4.027	4.027	4.021	4.013	4.002

Figure 17: Interpolated AXOD Data Set for Three-spool Low-pressure Turbine

This program has similar limitation when it comes to producing VCR models so a similar approach was taken as ws done with the TD2 program. Each spool was created and model as it's own spool to overcome AXOD's inability to handle spools rotating in opposite directions. It is harder to model off design conditions in AXOD as for each run the previous absolute flow angle changes along with the total pressure and total pressure. To account for this it was assume that only one turbine stage is varied at a time so that the inlet conditions are held constant as the VCR turbine runs through the off-design points.

```
ASU 3-SPOOL TURBINE HPT - TF 30,000ft MACH 0.5 Constant Test File
100 PERCENT SPEED
&DATAIN STAGE=1.,
TTIN=2100.,PTIN=78.6956,IAR=2,PTPS=1.2,DELC=.02,DELL=0.1,
DELA=0.0,FAIR=0.017,
STG=2.,SECT=3.,PCNH=2*0.333,0.334,VCTD=0.0,RPM=20000.,
RWG=5*1.0,EXPN=4.,EXPP=3.,SLI=0.0,DR=5*9.0,DT=2*10.0,3*10.5,
SDIA=3*0,SDEA=73.85,73.0,72.1
SETA=3*.88,SREC=3*1.0,SCF=3*.99,
RDIA=32.53,8.522,-15.92,
RDEA=75.809,75.904,76.065,
RETA=3*.87,RTF=3*1.0,RREC=3*1.0,RCF=3*.99,
ENDSTG=0.0 &END
&DATAIN STAGE=2.,
DR=5*9.0,DT=3*10.5,2*10.75,
RWG=5*1.0,
SDIA=64.645,63.173,61.973,SDEA=71.5,67.387,64.5
SETA=3*.88,SREC=3*1.0,SCF=3*.99,
RDIA=49.074,33.89,21.577,RDEA=67.879,68.549,68.926,
RETA=3*.91,RTF=3*1.0,RREC=3*1.0,RCF=3*.99,
ENDSTG=1.0, ENDJOB=1.0 &END

120 PERCENT SPEED
&DATAIN STAGE=1.,
PTPS=1.2,RPM=24000.,VCTD=0.,ENDSTG=0.0 &END
&DATAIN STAGE=2.,
ENDSTG=1.0, ENDJOB=0.0 &END
```

Figure 18: AXOD Input File for Three-spool High-pressure Turbine

5.2: Aircraft Flight Performance

It is important to understand the impact of power extraction on thrust and fuel flow and how this alters operating limit its flight across the flight envelope of the UAV. In this study, we developed models to understand the performance degradation over the entire flight envelope of a notional UAV powered by both the two-spool and three-spool designs.

The five column data produced in NPSS was developed for each engine and power extraction level. Next, we sketched up a notional straight wing airframe; see Figure 13, and developed an aerodynamic performance model using EDET [18]; see Figure 19 on the next page. I developed "five column propulsion data" using the methods described above. Once I had aerodynamic and propulsion data, we could estimate kinematic performance across the flight envelope [19]; I developed "sky map" plots that we can use to compare the total flight envelope performance impacts of differing power extraction strategies.

EDET is a legacy FORTRAN code initially developed at Lockheed for NASA; it calculates aerodynamic data and it was later modified to run through the command prompt of modern PCs [18]. EDET estimates the drag coefficient values of an aircraft at a range of altitudes, Mach numbers, and angles of attack. EDET calculates these drag coefficient values from a semi-empirical model that utilizes the broad geometry of an aircraft's wing, tails, and fuselage. EDET uses an equivalent-flat-plate model with complex form-factors and wetted areas to estimate skin friction drag [18]. It uses a simple quadratic basis to estimate induced drag. It also uses a

complex, empirical table lookup, to estimate non-parabolic drag-due-to-lift and other stall, buffet and compressibility effects on aircraft drag.

```
* CONFIGURATION : NOTIONAL UAV FOR LUKE
* SREF (FT^2) AR        TC       SW25      TR
 200.         10.      0.12      0.0     0.30
*
* SWET_WING  %CAMBER  AITEK     TRU       TRL
 380.          0         1       0         0
*
* SWET_FUSE   FUSE_L   FUSE_LoD  SBASE    CPBASE
 225.          30       10.      0.0     -0.16
*
* CRUDFACTOR
 0.28
*
* REF_ALT  REF_MACH
 10000     0.5
*
* ADDITIONAL COMPONENTS
*   S_WET      LEN      TC/FR   DELTA_CD0
VTAIL
   50.        4.00    0.10    0.000000
HTAIL
   50.        4.00    0.10    0.000000
```

Figure 19: Nominal UAV Dimension and EDET Input File

The UAV aircraft features an unswept wing (AR=10) wing with a nominal wing loading of 20-lbm/ft^2. Thus, the aircraft has Sref= 200-ft^2, b=44.72-ft, and c=4.47-ft. The wing section is 15% thick and has nominal camber (i.e. the wing is lofted with a section reminiscent of a NACA 23015). The fuselage is 30-ft long and has a fineness ratio of 10. The vertical tail has a planform area of ~25-ft^2. The horizontal tail has a planform area of ~45-ft^2. The empennage airfoils are 12% thick. The "crud" or excrescence drag factor is 28% of the basic zero lift drag estimate.

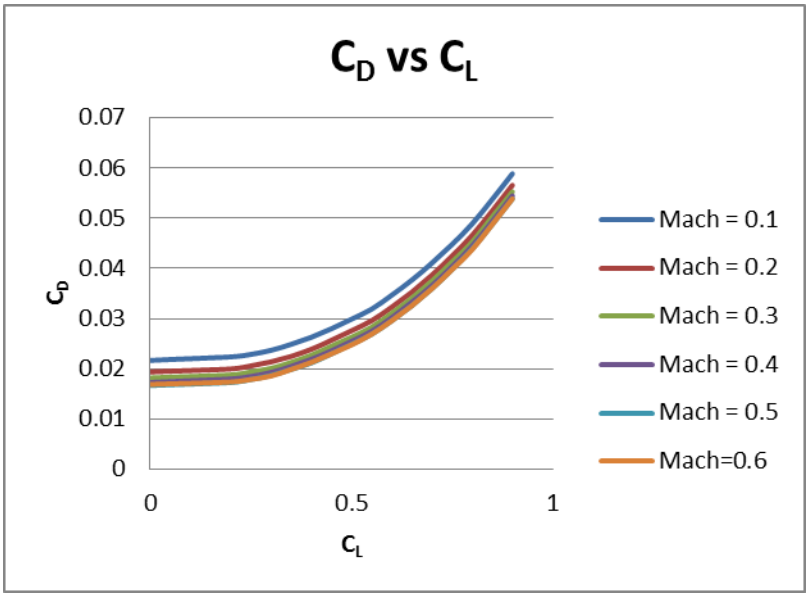

Figure 20: EDET Output for Drag Polar for the Nominal UAV Designed for This Study

To determine the performance of the specified aircraft and engine together at varying altitudes and Mach numbers, we use a point performance tool to develop "skymap plots." [19]. This code utilizes the aerodynamic data of EDET and the five column propulsion data, interpolating this data to develop contour plots of relevant aircraft performance metrics all as a function of speed and altitude. For our performance trade studies, the range for altitudes is set to 0-ft to 48,000-ft in increments of 1,000-ft and the range for Mach number is set to 0.0 to 0.6 in increments of 0.01 for all performance tests.

The most important performance value that is calculated through *Skymaps* is the specific range of the aircraft. Specific range is the efficiency of how much fuel is burned for every nautical mile travelled (nM/lbm); a higher value indicates a lower fuel burn per unit flight distance. Knowing the altitude and Mach number when the *SR* value is the highest allows for one to determine how fast and where the aircraft should be during most of its flight in order to burn

its fuel as efficiently as possible. The Specific Range is a metric that allows one to determine how much fuel is needed for a flight with the knowledge of how many nautical miles the aircraft needs to travel. Analysis of the Specific Range *Skymaps* for each chosen engine and aircraft combination is the main focus of our flight performance envelope trade study when we determine the effective performance of each engine.

Another important performance value is the endurance fuel flow of the aircraft. Endurance fuel flow *FF* is a metric of how much fuel is burned per unit time (lbm/hr); a lower value indicates increased endurance capability. Knowing the altitude and Mach number when the FF value is the lowest allows one to determine how fast and where the aircraft should be during most of its flight in order to maximize its time aloft.

Flight performance also requires an aircraft to climb. The unaccelerated rate-of-climb (ROC) is a metric of how rapidly the aircraft can change altitude without changing its true airspeed; a higher value indicates stronger climb rates. An aircraft responsive to Air Traffic Control commands should be able to attain at least a 500-ft/min climb rate.

Chapter 6 Methodology

This section details the evolution of this thesis from the original plans all the way to the final models and the results presented here.

The initial plans for this thesis involved designing a traditional two-spool turbine and a separate VCR free turbine that would come directly after a two-spool turbine. The free turbine would be used solely for power extraction for the onboard systems. The two-spool design went through the scaled NPSS model to get the pressure, temperature, mass flow, and power required for beginning the design process stated in the earlier sections. The original VCR model would use the same compressors.

The originally UAV mission concept was to fly at 10,000-ft at Mach 0.5 while producing 500 lbf of thrust (as a close-air support platform). It was designed to be a 4-stage two-spool design pushing 5.55 lbm/s through the core of the engine. The exit conditions from the first designed at the design point were then used for designing the VCR free turbine. The VCR turbine was designed to extract 50-HP from the flow at the design point. Both turbine stages geometry and blade angles are seen in Table 1.

Table 1: Initial Three-spool Geometry and Blade Angles

	Exit Hub Radius	Exit Tip Radius	Inlet Angle	Outlet Angle
Stator 1	3.25	4.0	0.0	73.0
Rotor 1	3.25	4.1	39.4	74.5
Stator 2	3.25	4.15	59.6	72.5
Rotor 2	3.25	4.6	43.1	72.9
Stator 3	3.25	4.6	52.3	72.8
Rotor 3	3.25	4.6	34.0	78.0
Stator 4	3.25	5.0	66.1	69.3
Rotor 4	3.25	5.5	22.5	72.0
VCR 1	3.25	5.5	30.4	47.3

The two-spool section was run through AXOD program varying the RPMs for each spool ranging between 120%-20% of the design RPM in increments of 10%. The data from AXOD was then interpolated between specific pressure ratios that when entering the data into a NPSS input file all the values would be for consistent pressure ratios. The two-spool section data was inputted into the NPSS program initial to validate that the model would properly converge and run through all the desired altitudes and Mach numbers.

The initial standard two-spool design properly converged for all altitudes and Mach numbers; the next task was to modify the NPSS model to include an additional spool and turbine. The addition of the simple VCR to the two-spool engine caused the model to fail. The reason for such failures most likely stemmed from NPSS being unable to balance the torque applied to the free turbine from the flow and the power extraction. Considerable effort was expended attempting to trick the model into accepting the new turbine. The initial plan was to apply a torque load the free turbine. This plan worked only when the torque load was kept constant, but if the torque load was kept constant, the power would fluctuate and was not the desired outcome. An attempt

was made to make the torque load vary with the free turbine RPMs, but this caused the program to become under constrained and the model failed to converge for any of the off design points.

The next attempt was to put a fictitious compressor attached to the free turbine. This was done to apply a secondary torque load to the free turbine to help constrain the model. This fictitious compressor stage had a pressure ratio of 1.001 in order to minimize the overall effect it would have on the following stages. This initially worked and allowed the free turbine to converge on a solution when no extra power extraction was applied. This fictitious compressor required less than one horsepower to run and changed the burner exit pressure by less than 1%. When power extraction was applied to the free turbine, the program ended up failing to converge for any meaningful power extraction. This process did prove that the additional turbine and shaft were properly built into the NPSS model.

These thermodynamic model failures prompted a reevaluation of the project I realized that three-spool designs that incorporate VCR stages are rare and their impact on aircraft performance had not been investigated.

From this point, the two-spool design was kept as the baseline to be compared to. A more general UAV reconnaissance mission seemed more appropriate to document the loss of specific range associated with a three-spool VCR design. If the engine was sized for low altitude performance, any loss of thrust would render the airframe inoperable. With a larger engine and higher altitude reference point, the degradation in top speed, altitude, climb performance and efficiency with changes in technology and power extraction could be meaningfully evaluated.

The five column data that NPSS outputs was then converted to the proper format to be used in the *Skymaps* program. [19] [20]. The new, higher thrust engine required new turbine stages, blade angles, and new turbine maps for NPSS with the geometry and angle presented in Tables 2 and 3.

Table 2: Design Point for Two-spool Baseline Model

	Exit Hub Radius	Exit Tip Radius	Inlet Angle	Outlet Angle
Stator 1	4.5	5.0	0.0	73.0
Rotor 1	4.5	5.25	8.5	75.9
Stator 2	4.5	5.25	63.2	69.3
Rotor 2	4.5	5.375	51.7	60.7
Stator 3	4.5	5.5	58.8	70.9
Rotor 3	4.5	5.9	48.3	67.8
Stator 4	4.5	6.8	41.9	69.3
Rotor 4	4.5	7.7	28.73	73.5

The three-spool model has could not be model as one continuous model due to the fact that a VCR stage was going to be placed within the turbine. For the increased thrust the high-pressure turbine is required to produce 676-Hp, the low-pressure turbine needs to produce 131-Hp, and the fan-turbine needs to produce 580.03-Hp. Out of the three power requirements the low-pressure turbine is the best suited to be a single VCR stage. This allows two stator vanes to be removed and makes the three-spool design be approximately the same length as the traditional two-spool design since the other two turbines require two stages to extract the necessary horsepower. Table 3 contains the geometry and blade angles for the three-spool design. Both the high-pressure turbine and the fan turbine are designed to operate at 20,000 RPMs while the low-pressure turbine is meant to operate at 15,000 RPMs. These values along with the additional values obtained from the TD2 software was used to create AXOD input files and the data received from AXOD was then interpolated and used to generate a three-spool model in NPSS as

it does not use blade angles in the program it does not care if the different stages are counter-rotating. When initially running the three-spool model the program was unable to converge for more than a few off-design points, but when the initial design point was changed to the current 30,000-ft and cruise at Mach 0.4 the model was able to properly converge. The process was repeated with the new inlet conditions at the design point, but when running the program the angles and performance did not change more than a few percent so the models were kept the same. The results for both the traditional two-spool and three-spool models will be discussed in the next section.

Table 3: Three-spool Geometry for Design Point

	Exit Hub Radius	Exit Tip Radius	Inlet Angle	Outlet Angle
HPT Stator 1	4.5	5.0	0.0	73.0
HPT Rotor 1	4.5	5.25	8.5	75.9
HPT Stator 2	4.5	5.25	63.2	68
HPT Rotor 2	4.5	5.375	33.9	68.5
LPT VCR	4.5	6.5	-10.5	70.2
FANT Rotor 1	4.5	5.75	39.6	69.0
FANT Stator 2	4.5	6.8	11.2	60.3
FANT Rotor 3	4.5	7.9	2.3	62.6

Chapter 7: Results

7.1: Engine performance results

By using the design point for 450-lbf of thrust at an altitude 30,000-ft and Mach number of 0.3 the velocity triangles for the two-spool model are given below in Figures 21-24. As stated in Chapter 5.1, they were initially designed to have a degree of reaction of 50% to reduce the likely hood of separation. This was not the case as at time the flow became choked when trying to achieve symmetric velocity diagrams so the velocity diagrams are changed until the flow is no longer choked. This caused the second and third stages to have the main pressure drop across the stages to mainly be across the rotors while the fourth stage main pressure drop came across the stator vane.

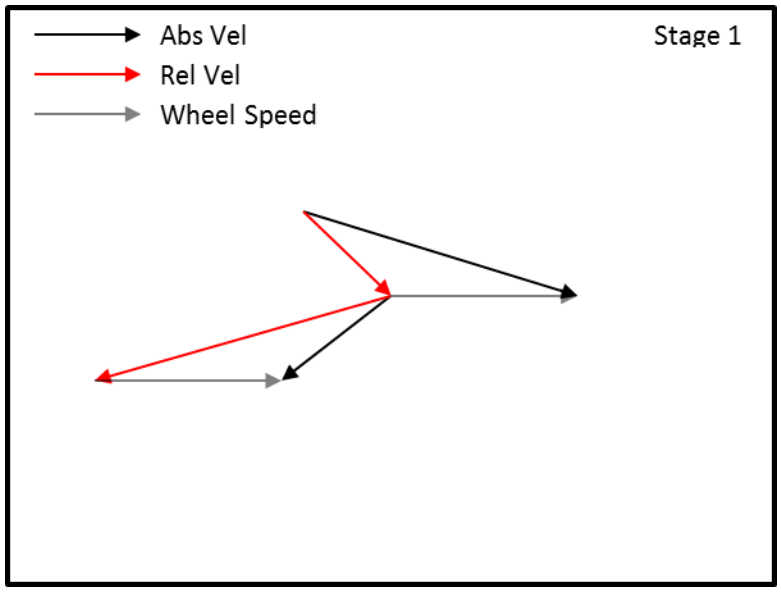

Figure 21: Stage 1 Velocity Triangles for Two-spool Design

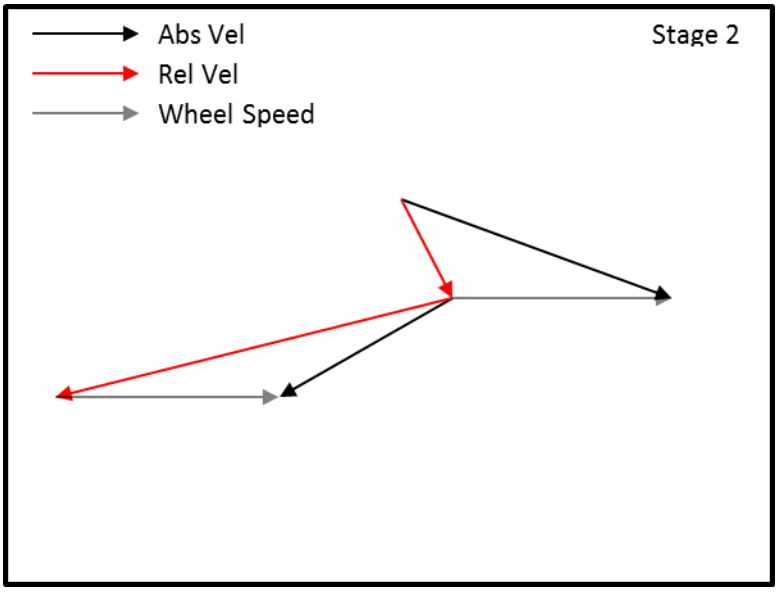

Figure 22: Stage 2 Velocity Triangles for Two-spool Design

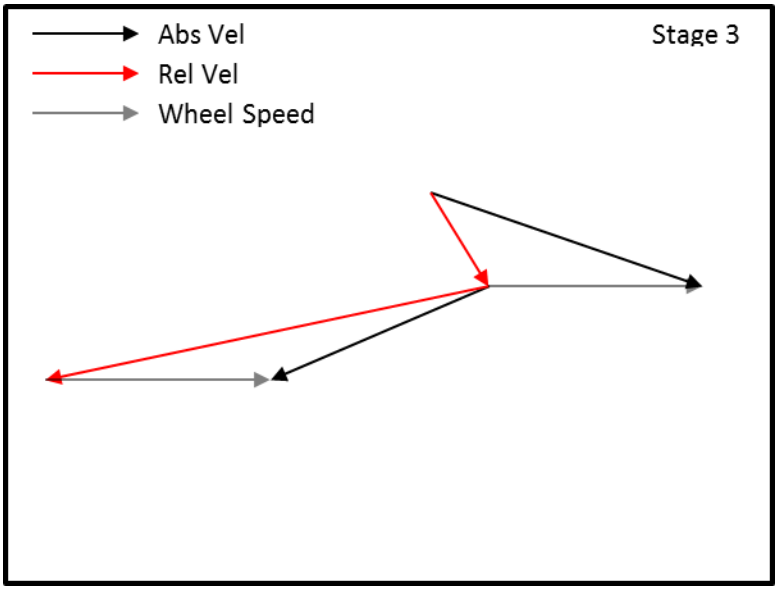

Figure 23: Stage 3 Velocity Triangles for Two-spool Design

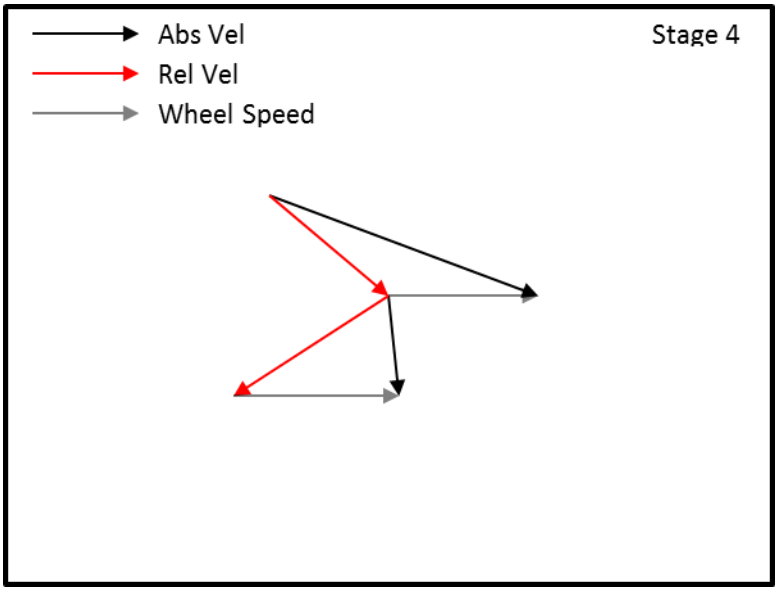

Figure 24: Stage 4 Velocity Triangles for Two-spool Design

For the three-spool design the first stage was kept constant as the inlet conditions were the same, but the second stage was changed to better set up the inlet flow angles that the VCR low-pressure turbine stage would see. With the additional stage placed in the turbine the fan turbine does not need to produce the same amount of work and required significant changes to the sizing and blade angles. The velocity triangles for all section can be seen in Figures 25-29.

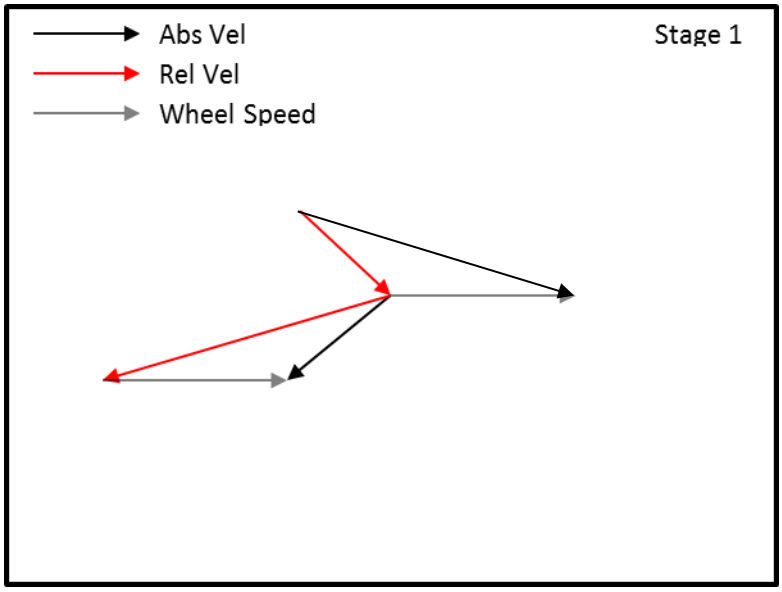

Figure 25: Stage 1 Velocity Triangles for Three-spool Design

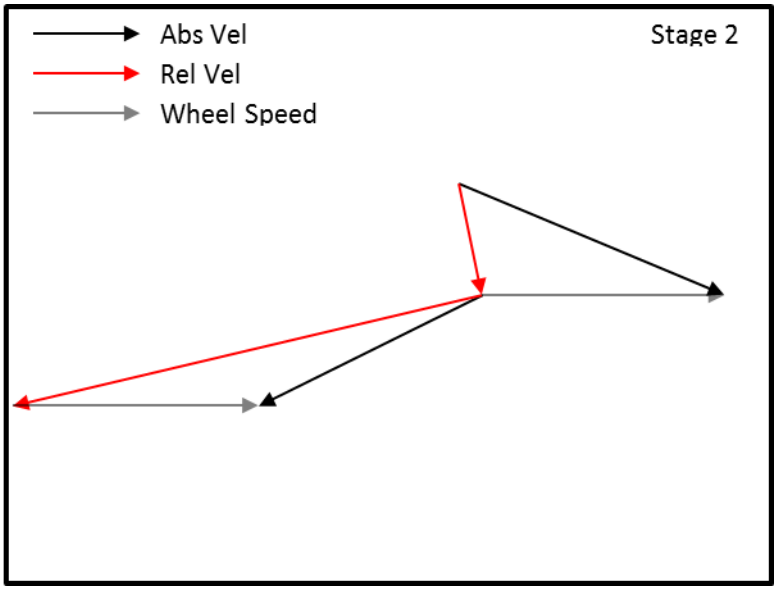

Figure 26: Stage 2 Velocity Triangles for Three-spool Design

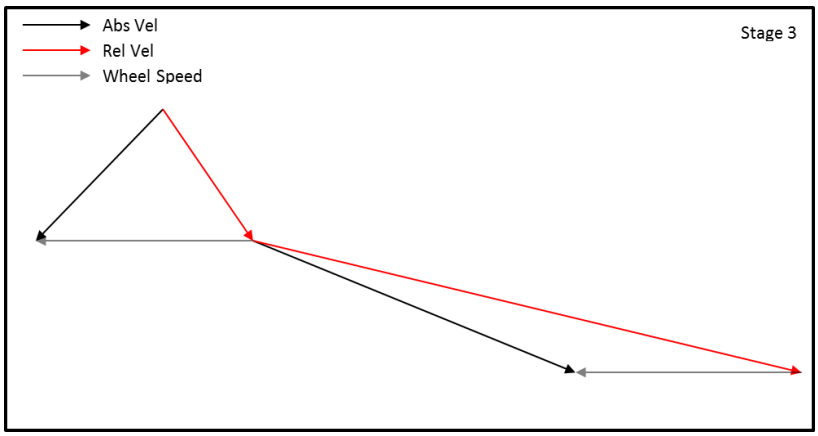

Figure 27: Stage 3 Low-pressure VCR Velocity Triangles for Three-spool Model

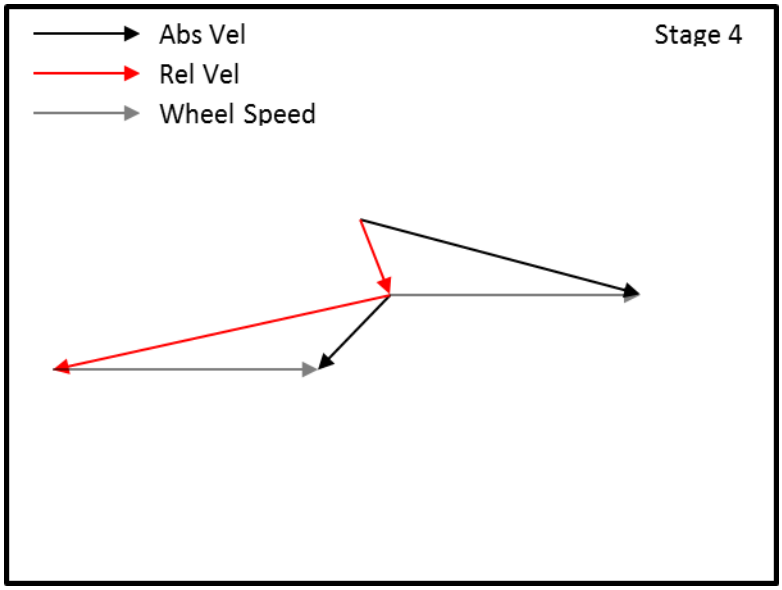

Figure 28: Stage 4 Fan Turbine Velocity Triangles for 3-spool Design

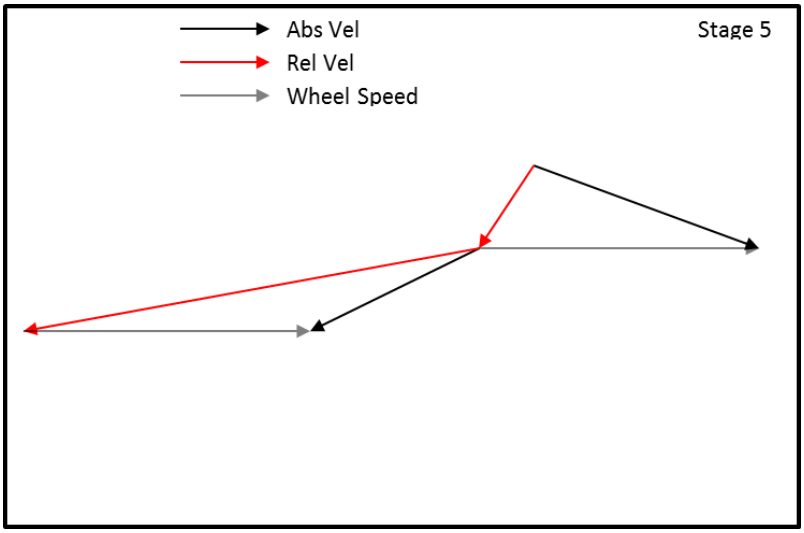

Figure 29: Stage 5 Fan Turbine Velocity Triangles for 3-spool Design

The results for each spool on both designs are presented in Table 4, below. The overall efficiency for the three-spool could not be directly pulled from the TD2 software and had to be calculated using Equation 8 using the exit total pressure and total temperature after the fan turbine stage (Station 5 in Brayton cycle) and the inlet conditions at the design point (Station 4 of the Brayton cycle). The calculation was done using the specific heat ratio of 1.35, as this is an average specific heat one would find within many gas turbine engines.

$$\eta_T = \frac{1 - \frac{T_{T5}}{T_{T4}}}{1 - \left(\frac{P_{T5}}{P_{T4}}\right)^{\frac{\gamma-1}{\gamma}}} \tag{8}$$

Table 4: Design Point Spool Comparison at Mach 0.5 at an Altitude of 10,000-*ft*

	2-spl HPT	2-SPL LPT	2-SPL Overall		3-SPL HPT	3-SPL LPT	3-SPL FANT	3-SPL Overall
Pressure ratio	3.41	5.45	18.58		3.40	1.28	3.91	17.01
Power extracted	676	711	1387		676	131	580	1387
Total efficiency	0.82	0.84	0.87		0.85	0.89	0.87	0.87

The power hooks for the two models show similar thrust lapse trends with slight variations when no extra power is extracted, the difference becomes more pronounced at higher altitudes with the three-spool model having higher TSFC values as seen in Figure 30.

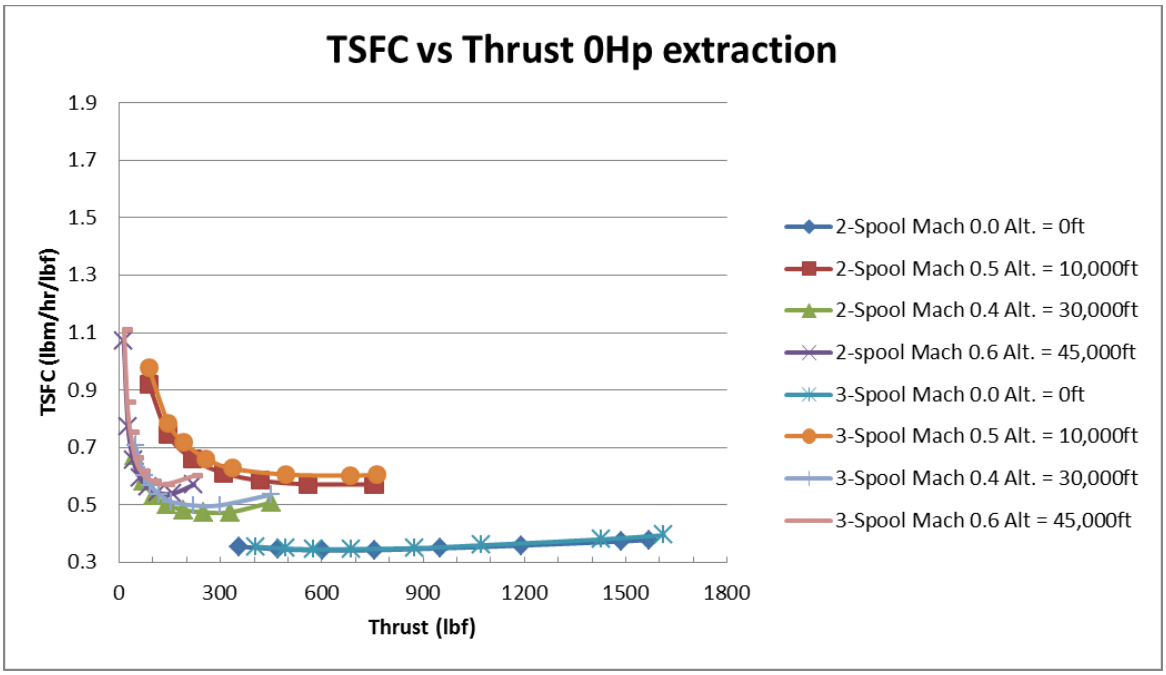

Figure 30: Power Hook for Both Models at Various Flight Conditions with No Power Extracted from Any Spool

When power is extracted from the two models low altitude data varies only slightly. The main difference comes when power is extracted from the low-pressure turbine. When power is extracted from the low-pressure turbine for the three-spool model the low power settings end up changing small amounts from previous settings. This trend hold trues for all the altitudes and flight conditions as seen in Figure 32. When power is extracted from the fan turbine, the fuel consumption greatly increases at the low power settings and the thrust falls off at these low power settings at higher altitudes. The fan is the main contributing factor to the overall thrust so

when the power is removed from that spool the fan overall performance degrades and the trust significantly falls off and the core is forced to compensate for the lost thrust by using large amounts of fuel.

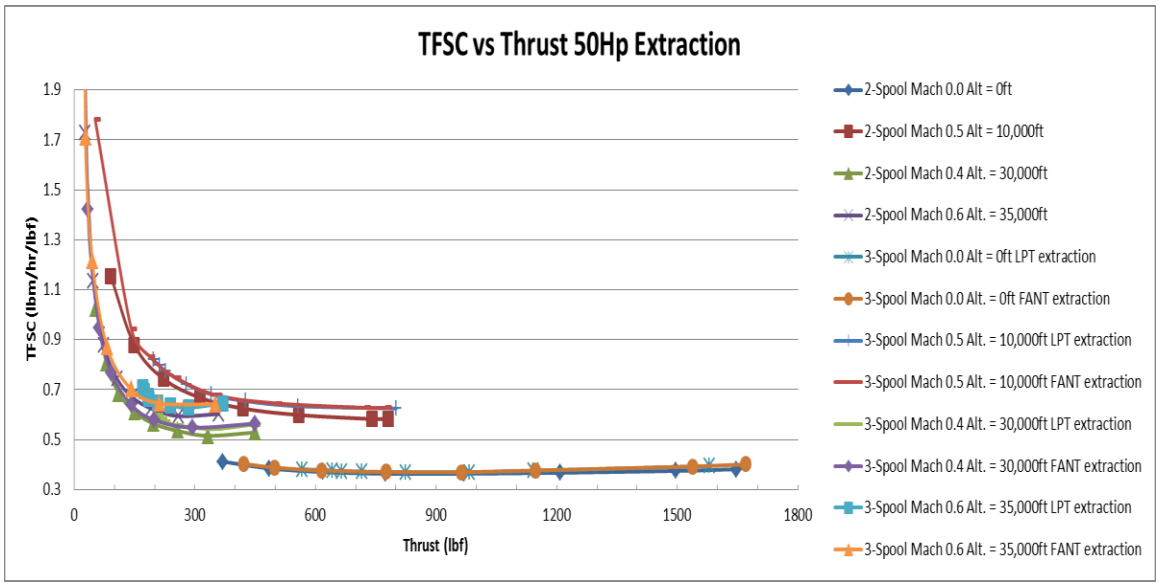

Figure 31: Power Hook for 50-Hp Extraction for Both Models at Various Flight Conditions

When 100-Hp is extracted from the models, the low altitude cases maintain similar trends as 50-Hp extraction with only a slight increase TSFC over the 0-Hp extraction case. As altitude and flight speed is increased, the low power settings for the three-spool model has significant fuel consumption increase when power is extracted from the fan for similar reasons as mentioned earlier. The three-spool low-pressure turbine extraction exhibits a similar trend of low power settings producing little variation in the thrust and producing a higher minimum thrust as seen in Figure 32.

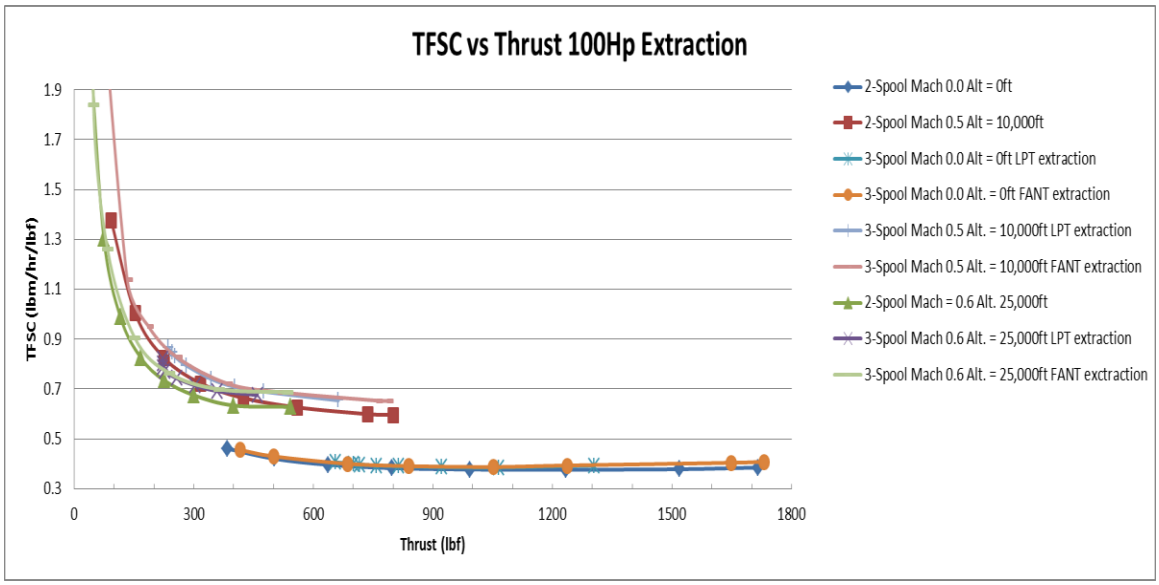

Figure 32 Power Hook for 100-Hp Extraction for Both Models at Various Flight Conditions

7.2: *Flight Envelope Performance*

Beginning with the design point comparison of both types of engines it is clear they are very similar to one another, but that the two-spool design has slightly better performance than the three-spool when it comes to more operating points it can fly at. It also has better specific range across the entire flight envelop. They do not have any specific difference when it comes to the rate of climb however.

Figures 33-38 depict the specific range (SR), max aerodynamic performance efficiency M(L/D), and max rate of climb (ROC) for each technology; with the two-spool design has a small region having a max specific range of 2.2-2.3 at about Mach 0.4 at an altitude of 44,000-ft. The three-spool design only has a max specific range of 2-2.1, about 5% worse.

The two-spool design also produces slightly more thrust at low altitudes and speeds, which allows the aircraft to successfully fly at such conditions. The three-spool design is slightly more limited and unable to fly as slow and as low as the two-spool design.

The additional spool generates another point for irreversibility to occur and is the most likely cause of such a difference. Based on the results provided two-spool designed is better for zero power extract this is rarely the case though in actual flight conditions.

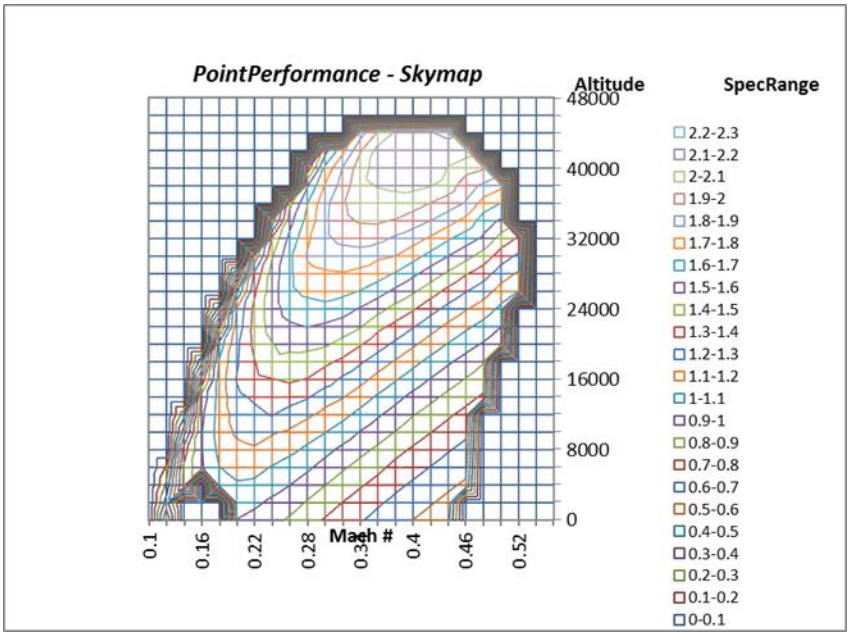

Figure 33: Two-spool Design Specific Range with 0-Hp Extraction

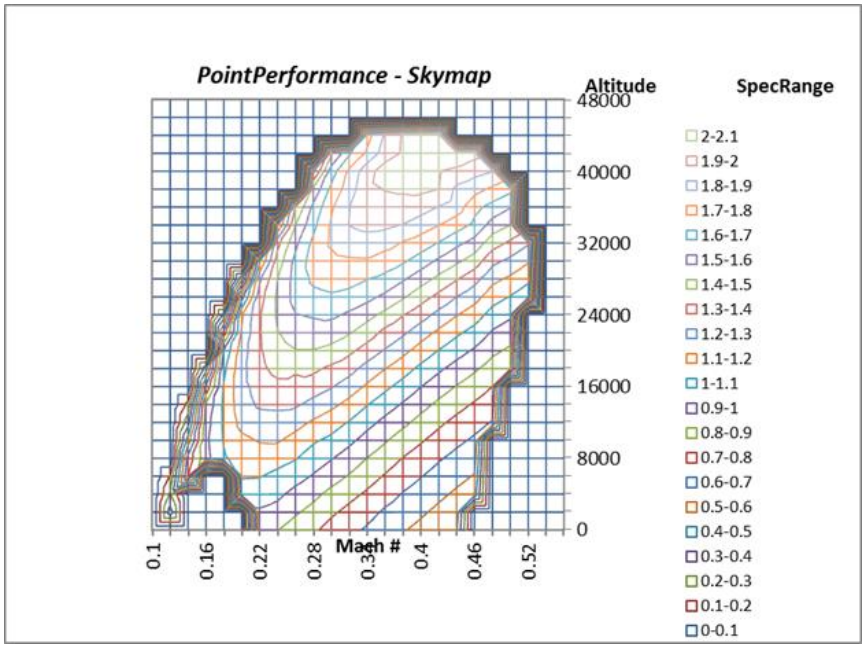

Figure 34: Three-spool Design Specific Range for 0-Hp Extraction

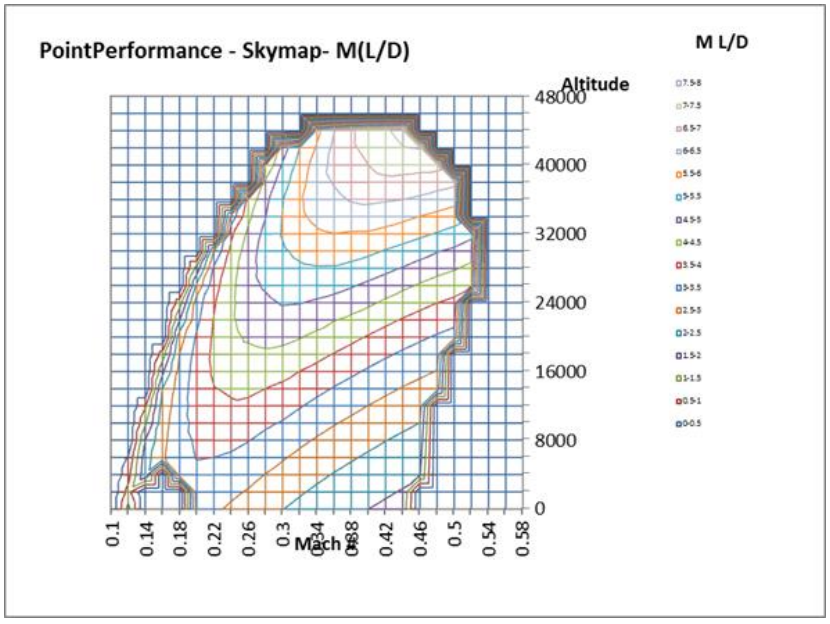

Figure 35: Two-spool Design Max L/D for 0-Hp Extraction

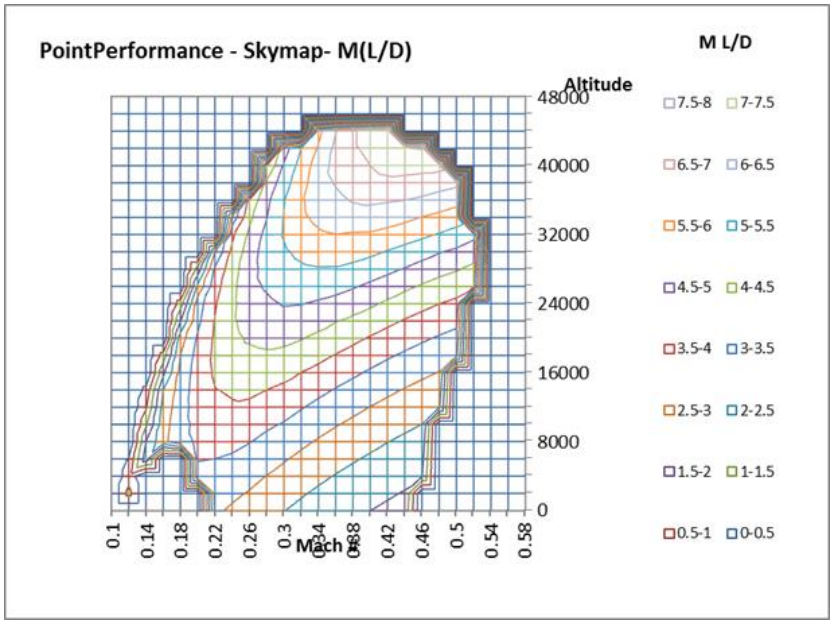

Figure 36: Three-spool Max L/D for 0-Hp Extraction

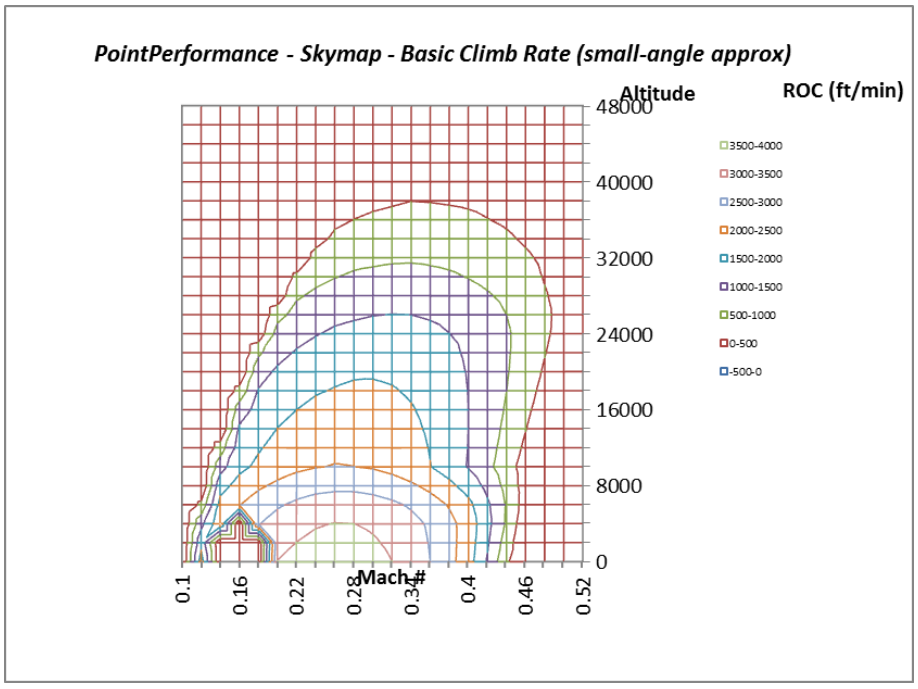

Figure 37: Two-spool Rate of Climb for 0-Hp Extraction

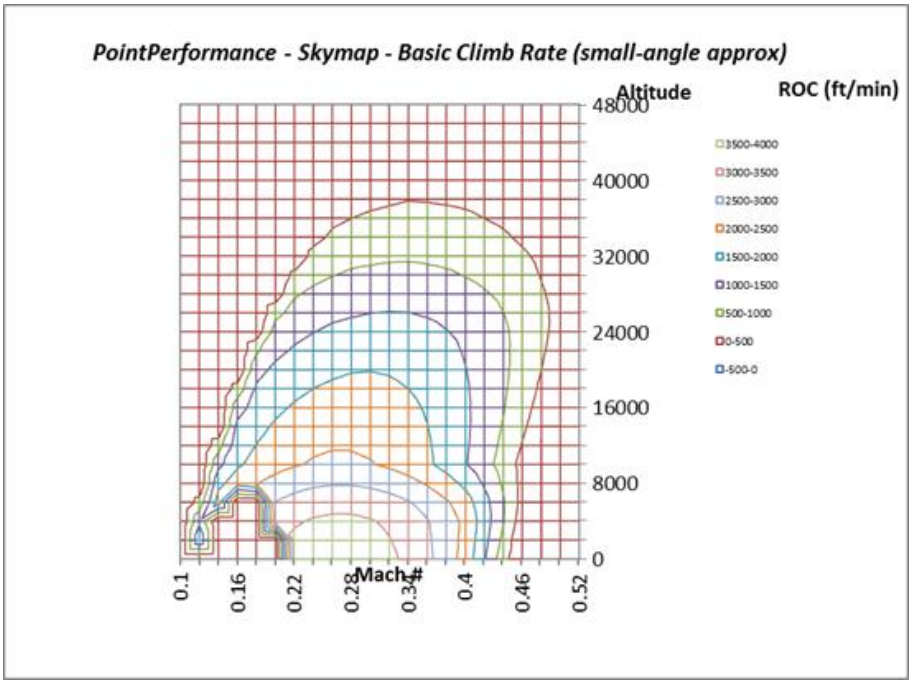

Figure 38: Three-spool Rate of Climb for 0-Hp Extraction

As stated earlier previous work was done on which of the spools for two-spool design is best suited for power extraction and found that the low-pressure spool is best suited for power extraction. No comparison between the two high-pressure spools can be made because of the previous work so only the two low-pressure turbines and the fan turbine will be compared for power extraction. The three-spool design performance for 50-Hp extraction from the low-pressure turbine loses all low speed performance and limits the systems flight speed to speeds greater than Mach 0.28, but is able to fly at the same altitudes as the two-spool designs. When power is extracted from the fan turbine the low speed performance is preserved, but at the cost of altitude performance and is capped 30,000-ft less than the two-spool design. The specific range also is slightly reduced when power is extracted from the fan turbine as well when compared to the power extracted from the low-pressure turbines. The reason for the reduced specific range is

being reduced is that the fan is being affected negatively which greatly reduces the efficiency of the fan. It is better to pull power from the fan spool even with the loss of altitude, because the lost in low speed ability means the UAV is unable to land and renders the design inoperable. Figures 39-47 display the *Skymaps* results for the power extracted from various spools for both engine models.

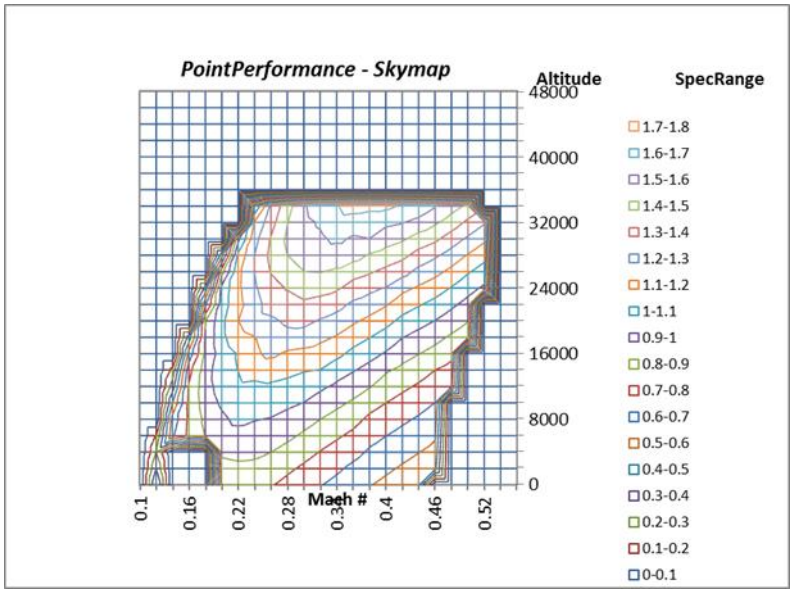

Figure 39: Two-spool Specific Range for 50-Hp Extraction

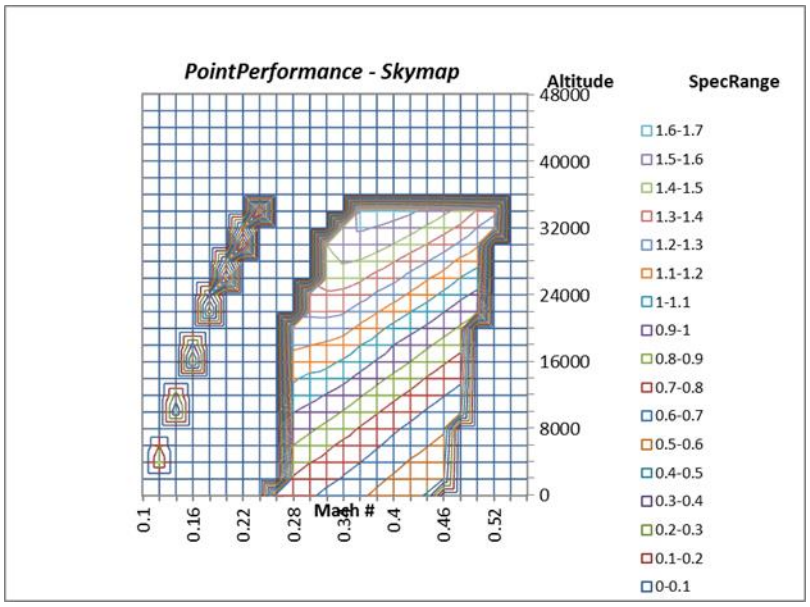

Figure 40: Three-spool Specific Range for 50-Hp Extraction from Low-pressure Spool

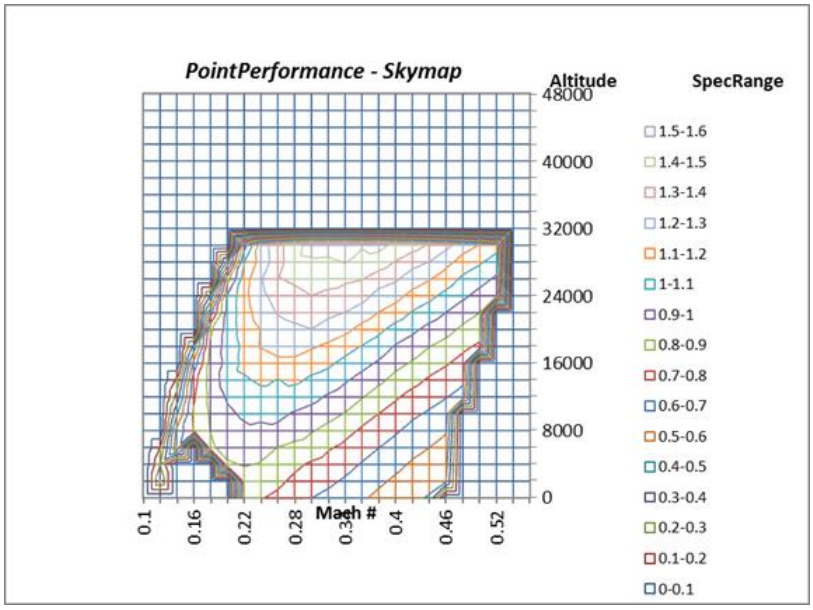

Figure 41: Three-spool Specific Range for 50-Hp Extraction from Fan Spool

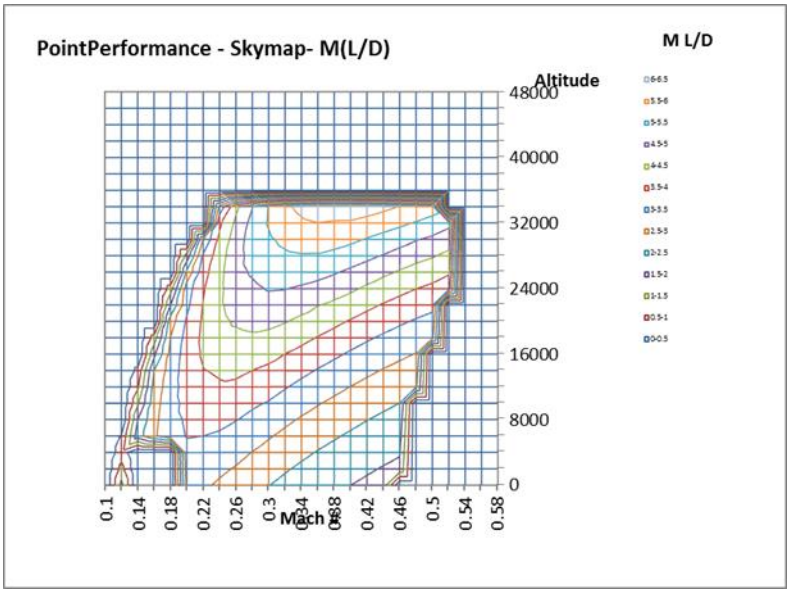

Figure 42: Two-spool Max L/D for 50-Hp Extraction

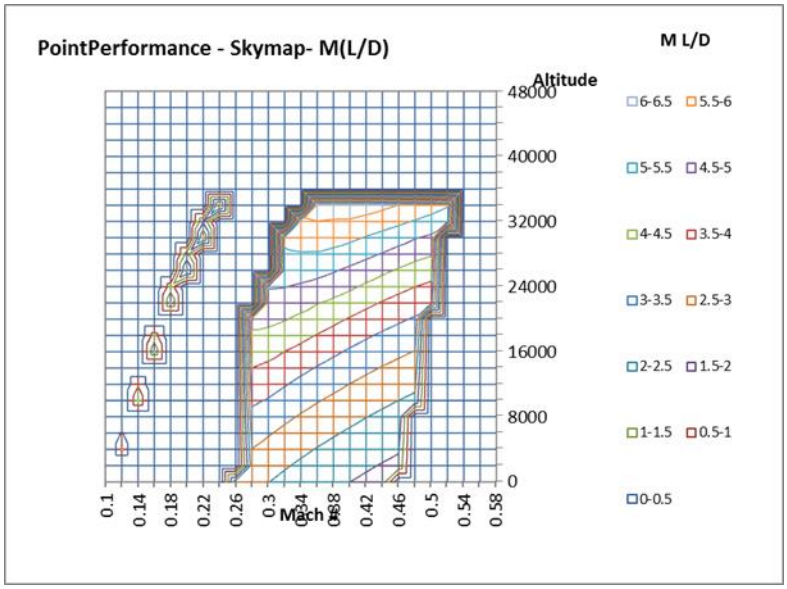

Figure 43: Three-spool Max L/D for 50-Hp Extraction from Low-pressure Spool

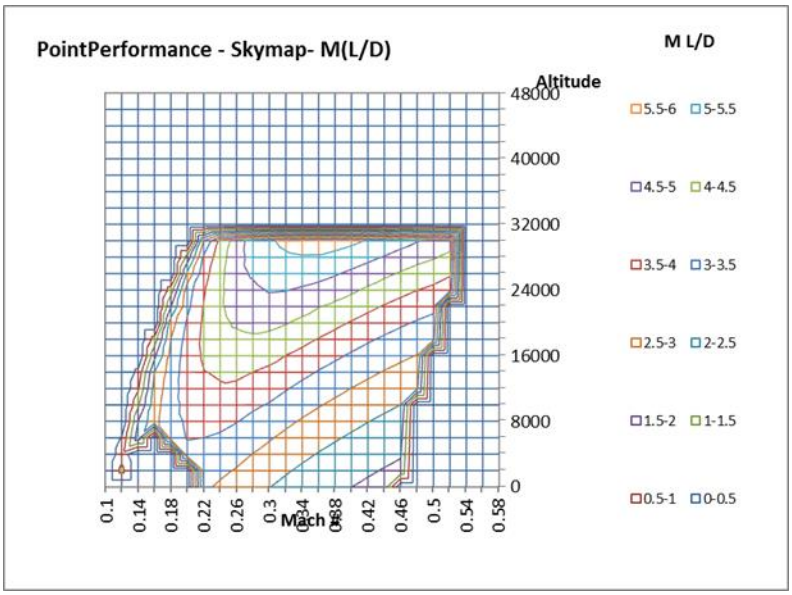

Figure 44: Three-spool Max L/D for 50-Hp Extraction from Fan Spool

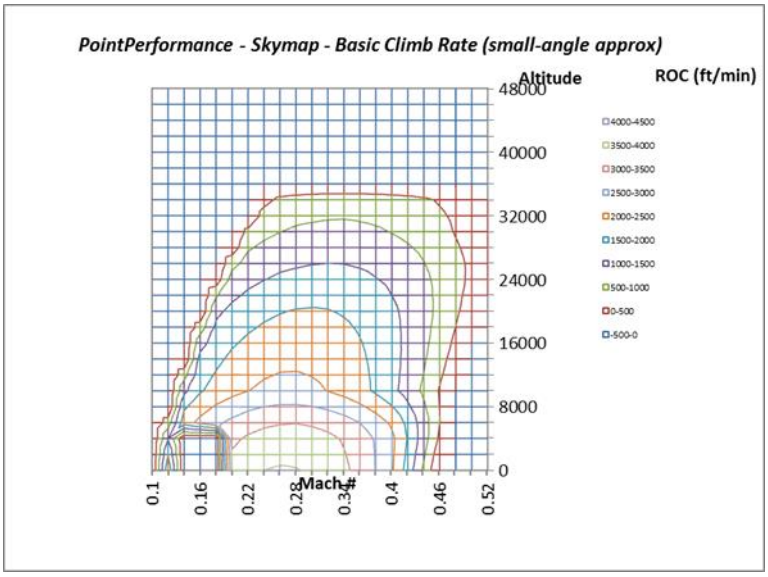

Figure 45: Two-spool Rate of Climb for 50-Hp Extraction

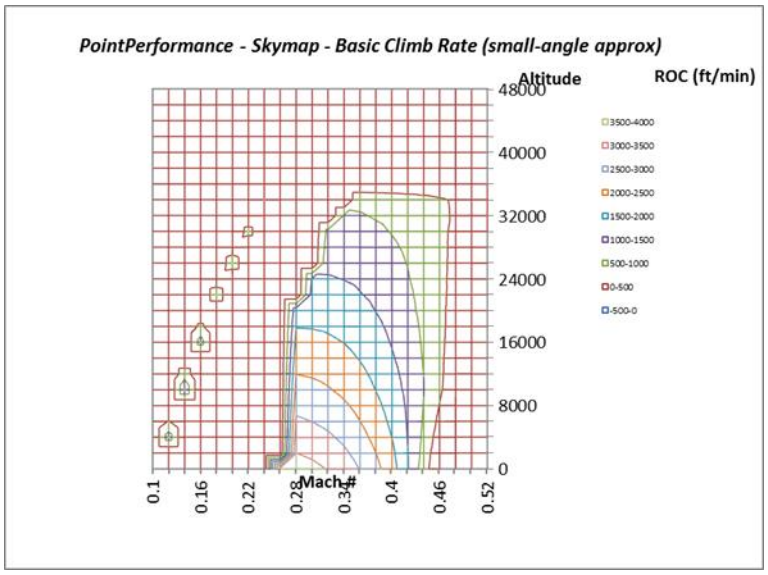

Figure 46: Three-spool Rate of Climb with 50-Hp Extraction from Low-pressure Spool

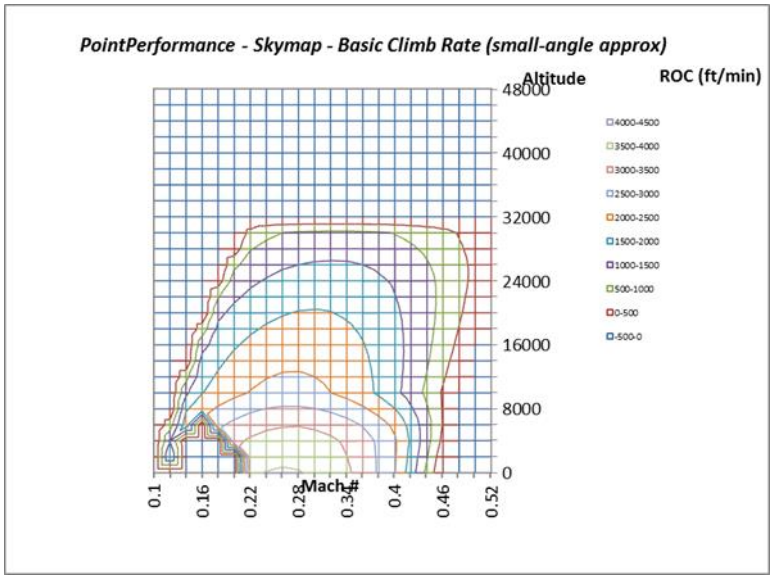

Figure 47: Three-spool Rate of Climb for 50Hp Extraction from Fan Spool

At 100-Hp extraction for all the scenarios, the maximum altitude is capped at roughly 25,000-ft. There is a significant reduction in flight envelop for the three-spool design when power is extracted from the low-pressure turbine, with the minimum speed being roughly Mach 0.28. There is a small difference between the performance of the three-spool and two-spool

designs when power is extracted from the fan turbine of the three-spool design with what appears to be the beginning of instability at the lower speeds and signals the soon collapse of low speed performance as seen in Figure 51. The specific range of both engines is drastically reduced and nearly 50% of what it at 0-Hp extraction Figures 48-50.

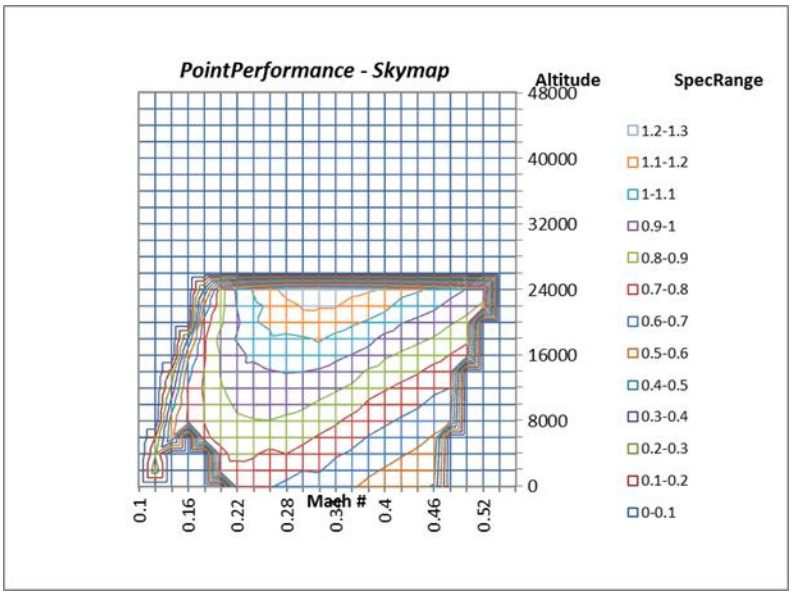

Figure 48: Two-spool Specific Range for 100-Hp Extraction

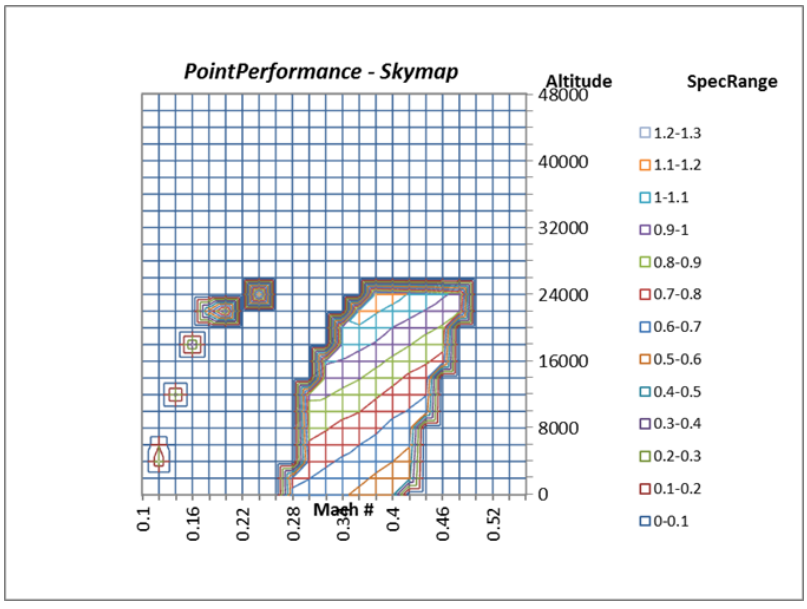

Figure 49: Three-spool Specific Range for 100-Hp Extraction from Low-pressure Spool

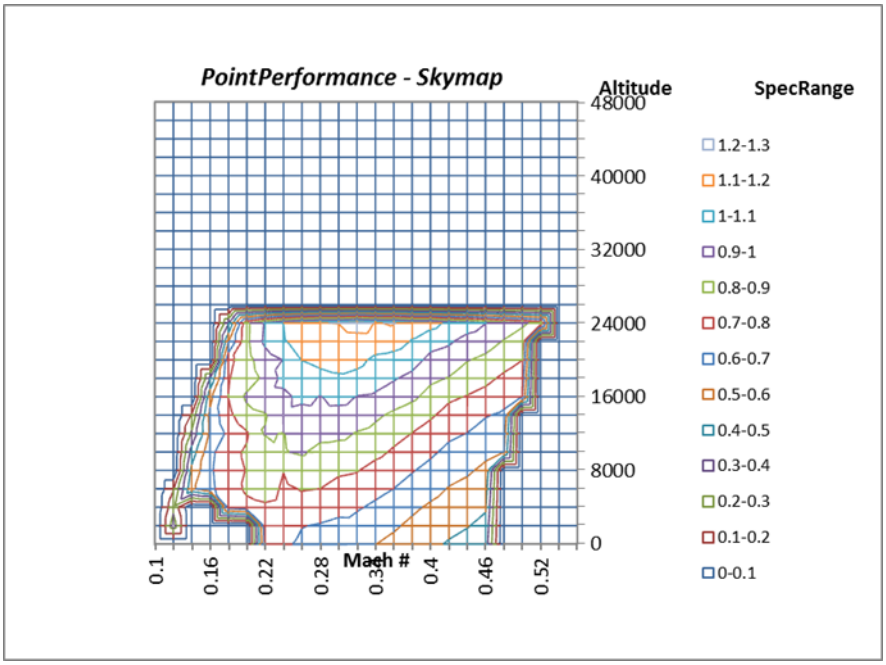

Figure 50: Three-spool Specific Range for 100-Hp from Fan Spool

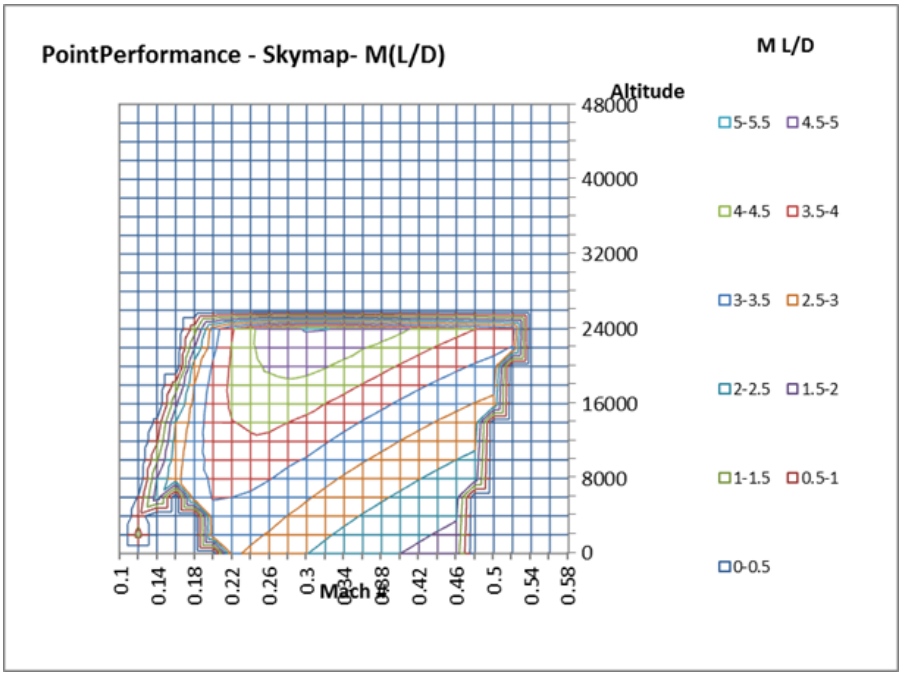

Figure 51: Two-spool Max L/D for 100-Hp Extraction

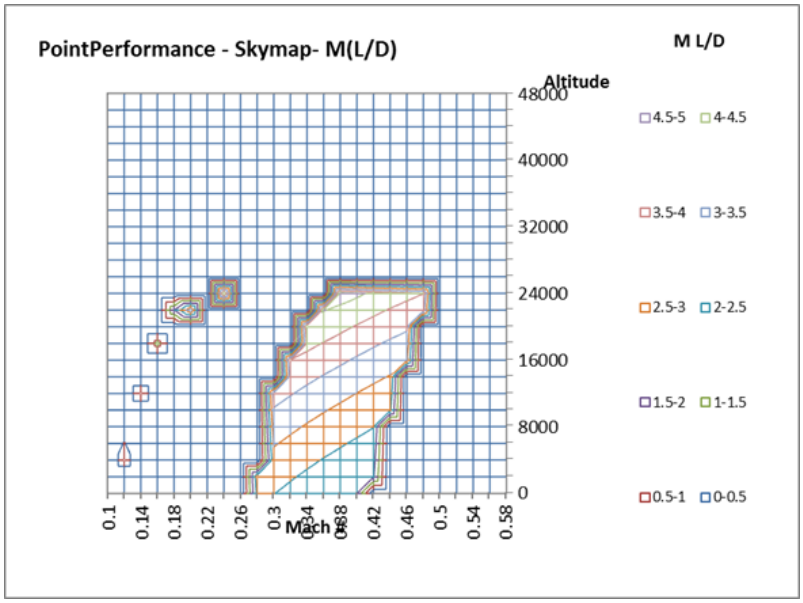

Figure 52: Three-spool Max L/D for 100-Hp from Low-pressure Spool

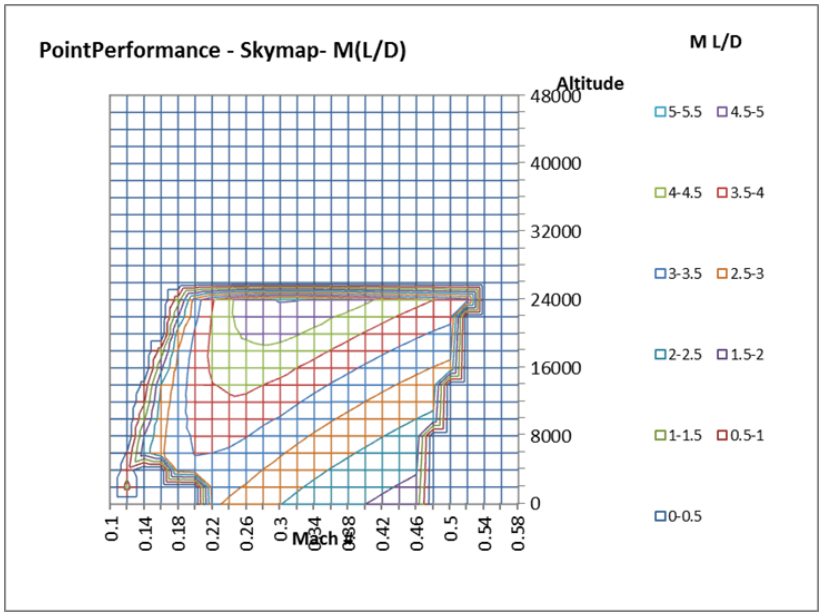

Figure 53: Three-spool Max L/D for 100-Hp from Fan Spool

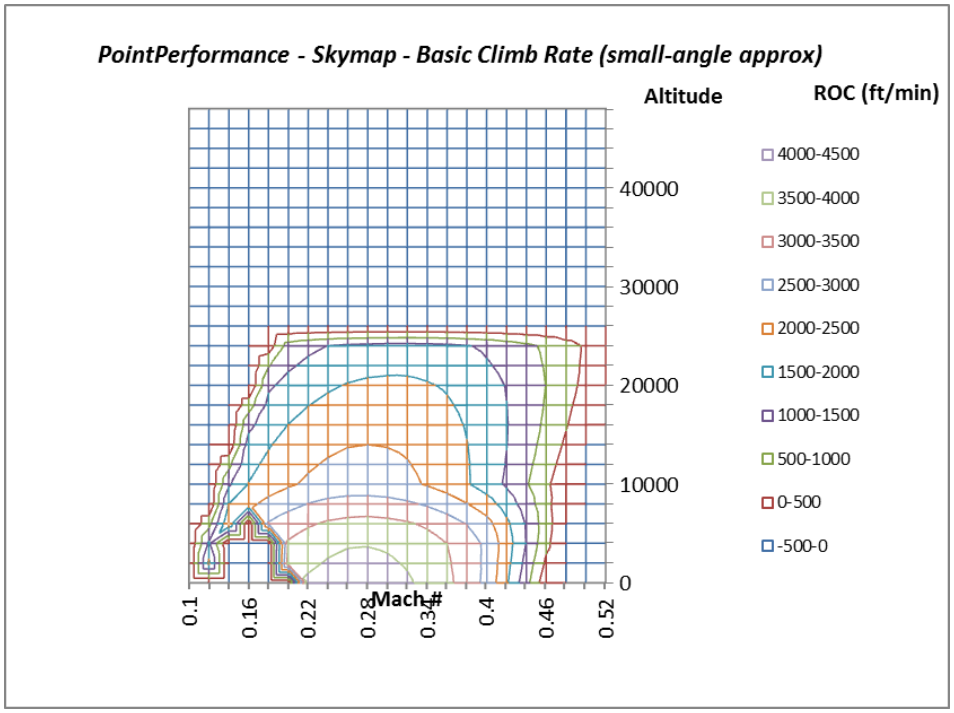

Figure 54: Two-spool Rate of Climb for 100-Hp

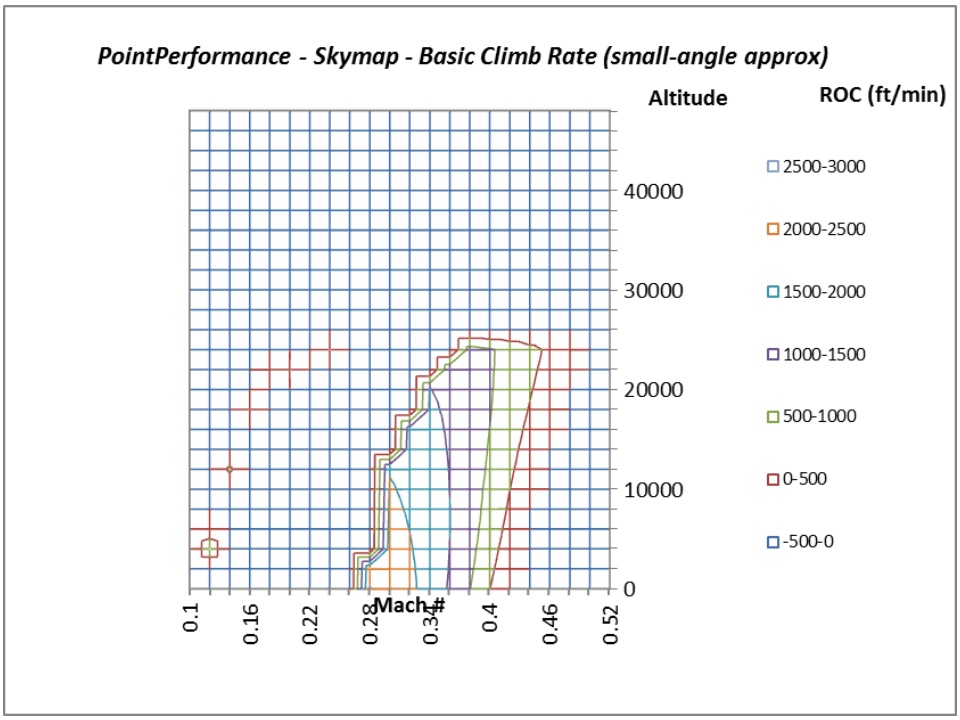

Figure 55: Three-spool Rate of Climb for 100-Hp from Low-pressure Spool

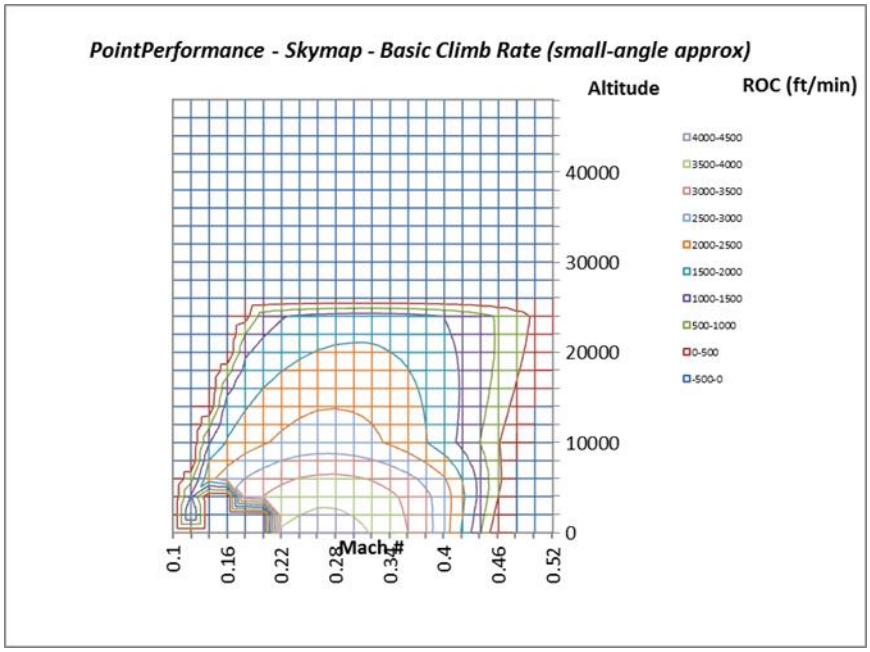

Figure 56: Three-spool Rate of Climb for 100-Hp from Fan Spool

Chapter 8: Discussion

From the data, it can be inferred that by decoupling the fan and the low-pressure turbine can actually hurt the overall performance of the engine. By decoupling the two the low power setting are severely affected. The three-spool low-pressure turbine's performance is affected significantly because the power that is being drawn off it is a significant percentage when compared to the power being drawn by the compressor. At the initial design point the low-pressure compressor required 506-Hp and the power extracted that was tested was 50-Hp and 100-Hp that is roughly 10% and 20% of the power so the turbine has to do a significant amount of extra work that it is not initially designed for. The low-pressure spool must compensate for this by forcing the low-pressure compressor to operate at a higher minimum RPM setting. These higher RPM settings correlate to a lower torque load in NPSS; Equation 9 gives the way the torque is calculated. For the same levels of thrust the low-pressure compressor, for the three-spool engine requires more power Figure 57 on the next page. These high RPMs also mean that the low-pressure compressor always imparts large amount of work to the flow this is the reason that the low power settings produces more thrust. The reason for the decreased performance when power extracted from the fan turbine section is that the fan produces the majority of the thrust. This forces the core to compensate and increases fuel consumption.

$$\tau = \frac{P * 550 * 60}{2 * \pi * N} \tag{9}$$

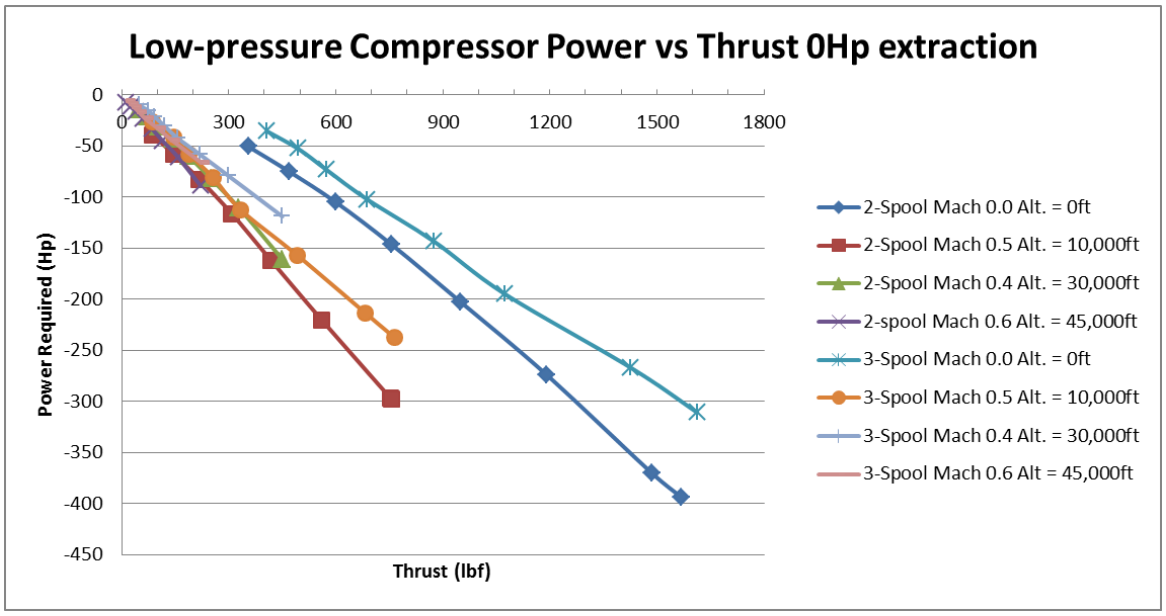

Figure 57: Low-pressure Compressor Required Power at Various Altitudes and Flight Speeds with No Power Extraction

The two-spool design is less affected by the power extraction because the extracted power is a smaller percentage compared to the power that the fan and low-pressure compressor combine require. This means that the three-spool design does not perform as well when power is extracted any of the spools when compared to the two-spool design, any power extracted from the engine should be done on the spool that normally requires the most power as the power extracted will have the minimal effect on the overall performance.

The three-spool design does allow for a unique possibility of extracting power from both the fan turbine and low-pressure turbine at the same time. By doing this though, the mechanical setup of the engine could become significantly complex and increase the cost of such a design. This method showed an improvement over the two-spool design and increased the altitudes at which the UAV can operate at with similar specific range.

By drawing power from both spools at the same time the low speed and low altitude performance is non-existent; such a method for power extraction could only be considered for high altitude operations; see Figure 58. There is notable improvement, however, when 50-Hp is extracted from the fan turbine and 50-Hp is extracted from the low-pressure turbine instead of extracting 100-Hp from either individual spool; see Figure 59. By extracting equally from both turbines the UAV gains the ability to continue operating up to 40,000-ft, a 16-000-ft improvement over the traditional two-spool design. This increase in altitude allows the range to vastly improve with the specific range having an improvement of nearly 30% over the power extraction methods. The low-speed performance is eliminated by doing this and limits the ability to fly at low-speeds with power extraction; this makes landings dangerous.

Uneven power extraction can greatly lead to improvement in the flight envelope of the UAV. Figure 60 shows the flight envelope when 25-Hp is extracted from the low-pressure turbine and the remaining 75-Hp is drawn from the fan turbine. The altitude improvement is up to 45,000-ft. It is worth noting that the specific range is optimal at higher speeds when the power is split this way. Surprisingly the altitude performance is better when compared to the three-spool performance and 50-Hp is extracted from the fan driven spool, but at the cost of fuel efficiency. The low-speed performance is better preserved compared to the other three-spool power extraction options that involve the low-pressure turbine, but still has a large unsafe low-speed region.

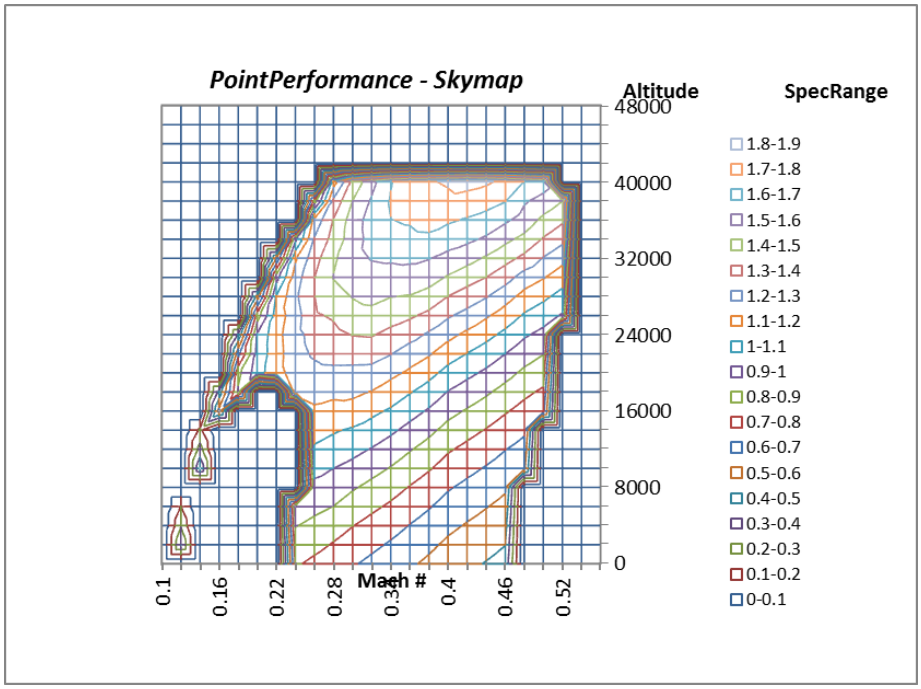

Figure 58: Specific Range of Three-spool Model with 25-Hp Extracted from the Fan Turbine and 25-Hp Extracted from the Low-pressure Turbine

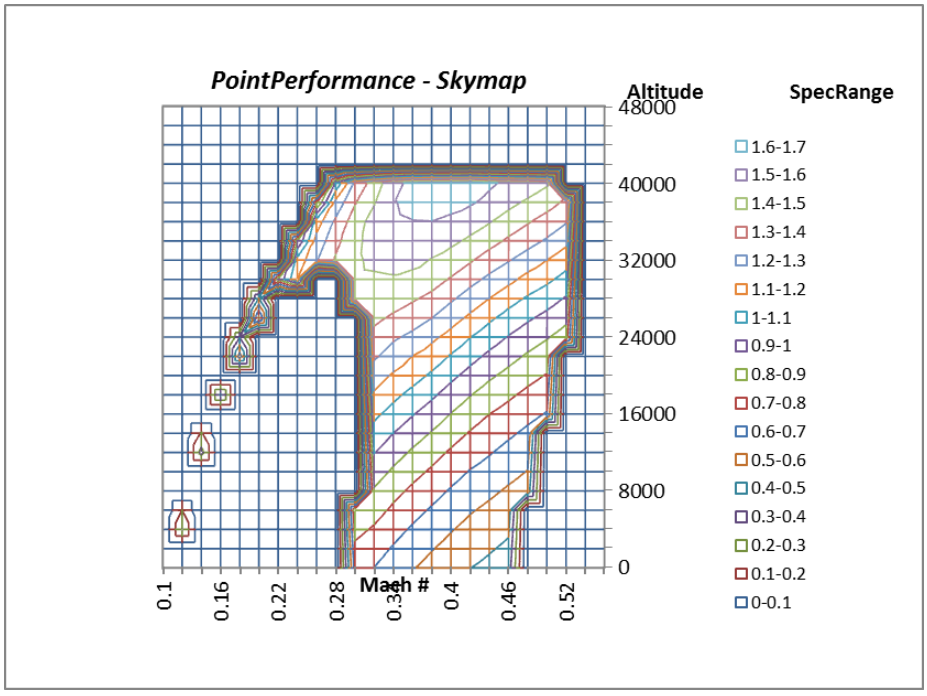

Figure 59: Specific Range of Three-spool Model with 50-Hp Extracted from the Fan Turbine and 50-Hp Extracted from the Low-pressure Turbine

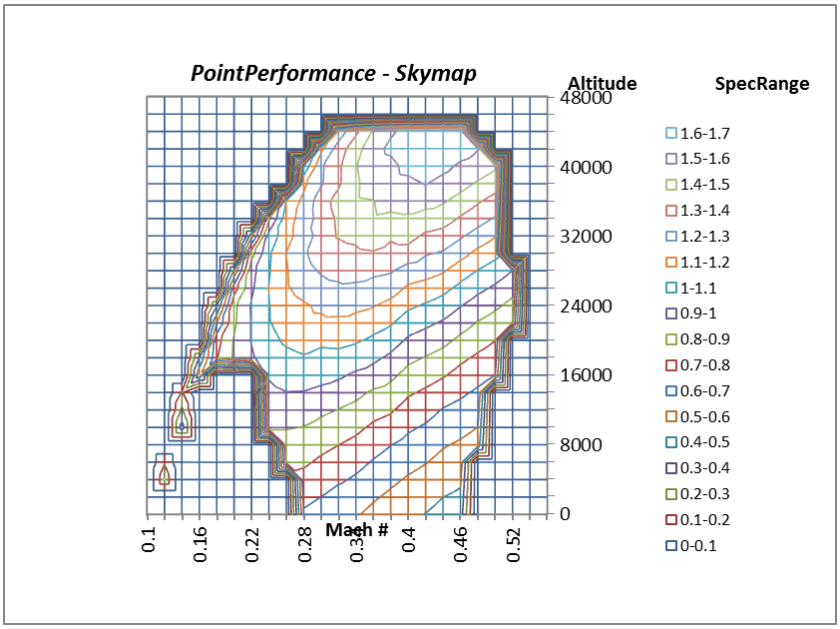

Figure 60: Uneven Power Extraction with 25-Hp from the Low-pressure Turbine and the Remaining 75-Hp from the Fan Turbine.

Chapter 9: Conclusion and Recomendations

This thesis work has shown that the low-pressure compressor is needed for low-speed flight; extracting power from it will eliminate the ability to operate at low-speeds. Power extraction from the fan turbine better preserves the flight envelope, at the cost of fuel economy. For a three-spool design to outperform a typical two-spool design, a complex system would need to simultaneously extract power from both the low-pressure spool and the fan spool. By doing this, the low speed performance is hindered by high idle thrust, but high speed and high altitude flight is better preserved.

Future work should look into seeing if the cost benefit of such a design along with the practicality of building such a complex gas turbine and dual spool power extraction system. For optimal performance 70-80% of the power demand should be drawn from the fan driven spool and the remaining amount be extracted from the low-pressure spool.

Because decoupling the fan from the low-pressure turbine actually degrades the flight envelope of a system when power is extracted any benefits of VCR would be eliminated. This system also operates in an environment that is not conducive to VCR technologies since the low-pressure turbine has to operate at high RPM settings to extract the required power and ensure the low-pressure compressor operates properly.

The original plan of developing a separate free turbine that is placed directly after a traditional two-spool design should still be investigated as it could operate in conditions that are better suited for VCR technology. Power extraction of such a system would no longer affect the

performance of the low-pressure compressor, preserving the low speed flight conditions, and the performance of the fan, preserving the fuel efficiency of the system. To do this alternative software that models entire propulsion systems would need to be used as NPSS was proven incapable of successfully modeling such a system.

Future works should also include compare a traditional three-spool design against a three-spool design incorporating VCR technology. This will allow for an analysis of the benefits of VCR technology for two identical engines. Studying the benefits of building VCR stages out of ceramics for both cost benefits and ability to withstand higher total inlet temperatures need to be under consideration for future studies. These future studies are need to have complete knowledge on VCR technologies and the feasibility of incorporating them into UAV engines.

REFERENCES

[1] N. Stone and T. Takahashi, *Aircraft Performance Impacts of Power and Bleed Air Extration on a COTS Engine Powered UAS AIAA 2019-1309,* Tempe, AZ: Arizona State University, 2019.

[2] The National Academies of Sciences Engineering Medicine, "Power Related Technologies," in *Uninhabited Air Vehicles*, Washington D.C., NAtional Academy Press, 2000, pp. 71-81.

[3] L. Moroz, P. Pagur, Y. Govorushchenko and K. Grebennik, "Comparison of Counter-Rotating and Traditional Axial Aircraft Low-Pressure Turbines Integral and Detailed Performance," in *International Symposium on Heat Transfer in Gas Turbne Systems*, Antalya, Turkey, 2009.

[4] "F119 Engine," United Technology company, [Online]. Available: www.pw.utc.com/products-and-services/products/military-engines/F119-Engine/. [Accessed 24 March 2019].

[5] W. Zhao, B. Wu and J. Xu, "Aerodynamic Design and Analysis of a Multistage Vaneless Counter- Rotating Turbine," *Journal of Turbomachineray,* vol. 137, no. 6, 2015.

[6] D. J. Dorney and K. L. Gundy-Burlet, "Effects of Hot Streak Shape on Rotor Heating in a High-Subsonic Single-Stage Turbine," NASA Ames Research Center, Moffett Field, 1999.

[7] Z. Qingjun, T. Fei, W. Huishe, D. Jianyi, Z. Xialu and X. Jinzhong, "Influence of Hot Streak Temperature Ratio on Low Pressre Stage of Vaneless Counter- Rotating Turbine," in *ASME Turbo Expo,* Montreal, Canada, 2007.

[8] W. T. Wintcuky and W. L. Stewart, "Analysis of Two-Stage Counterrotating Turbine Efficiencies in Terms of Work and Speed Requirements," Lewis Flight Propulsion Labratory, Cleveland, 1958.

[9] J. LuCheng, "Analysis of Technical Challenges in Vaneless Counter Rotating Turbomachinery GT2007-27617," in *ASME Turbo Expo*, Montreal, Canada, 2007.

[10] N. Cumpsty, Jet Propulsion A simple guide to the aerodynamic and thermodynamic design and performance of jet engines, New York: Cambridge University Press, 2011.

[11] NASA, "Ideal Brayton Cycle T-s diagram," NASA Glenn Research Center, [Online]. Available: https://www.grc.nasa.gov/www/k-12/airplane/brayton.html. [Accessed 25 March 2019].

[12] D. Hinch, "Concept NREC," NREC, 12 October 2018. [Online]. Available: https://www.conceptsnrec.com/blog/why-are-turbine-blades-twisted. [Accessed 25 March 2019].

[13] OpenWAM, "Turbine," OpenWam Manual, 10 Novemeber 2011. [Online]. Available: http://openwam.webs.upv.es/manual/index.php?title=Turbine. [Accessed 25 March 2019].

[14] Burbank, "Wikipedia," Wikimedia Foundation, Inc., 21 March 2012. [Online]. Available: https://en.wikipedia.org/wiki/File:Hpcompressorwl.gif. [Accessed 26 March 2019].

[15] Numerical Propulsion System Simulation Consortium, NPSS User's Guide, Numerical Propulsion System Simulation Consortium, 2016.

[16] Energy Service Group, *Vector Diagram,* Fountain Hills: ESG, 2017.

[17] A. J. Glassman, *User Manual and Modeling Impro,* Toledo: National Aeronautics and Space Administration, 1992.

[18] R. Feagin and W. Morrison, *Delta Method, An Emperical Drag Buildup Technique,* Burbank, CA: National Aeronautical and Space Administration, 1978.

[19] T. Takahashi, Aircraft Performance and Sizing Volume 1, New York: Momentum Press, 2016.

[20] T. T. Takahashi, "Aircraft Concept Design Performance Visualization Using an Energy Maneuverability Presentation AIAA 2012-5704," in *12th AIAA Aviation Technology, Integration, and Operation (ATIO) Conference and 14th AIAA/ISSM*, Indianapolis, 2012.